THE ASTROPHYSICAL JOURNAL, 481:132–156, 1997 May 20

SINKING SATELLITE DISK GALAXIES. I. SHELL FORMATION PRECEDED BY CESSATION OF STAR FORMATION

MAKOTO KOJIMA AND MASAFUMI NOGUCHI
Astronomical Institute, Tohoku University, Aoba, Sendai 980-77, Japan
Received 1996 May 20; accepted 1996 December 5

ABSTRACT

Detailed numerical simulations have been carried out on the sinking of a gas-rich disk galaxy into a large elliptial (spherical) galaxy. Both elliptical and spiral galaxies have been modeled as self-gravitating particle systems. The interstellar gas component in the disk has been modeled as a system of inelastic cloud particles dissipating kinetic energy in mutual collisions. Star formation processes and gas consumption owing to star formation are included in the numerical code. Sinking on a radial or slightly retrograde orbit has been found to produce regular shell structures (i.e., without loops or filaments) made from the disk material. In this shell formation, no significant segregation of the stellar and gaseous components occurs. Global distribution of the gas clouds is similar to that of the stars, though the latter make clearer shells. Star formation is turned off well before the shells develop, because gas clouds are widely scattered and the gas density is much decreased. We propose that the "poststarburst" nuclei often observed in shell galaxies are not necessarily the result of preceding starbursts, as is widely believed, but could be the result of this drastic truncation of star formation activity.

Subject headings: galaxies: interactions — galaxies: ISM — galaxies: kinematics and dynamics — galaxies: starburst — galaxies: structure

1. INTRODUCTION

Elliptical galaxies often possess peculiar properties that are thought to be the outcome of the accretion of small companion galaxies. They include shell (or ripple) structures, kinematically distinct cores, and dust lanes. Among these peculiarities, shells or ripples have attracted much attention recently and promoted many observational and theoretical studies. Statistics based on deep photometry suggest that a large fraction of elliptical galaxies possess shells or ripples, although the intensity and morphology of these structures are widely varied. The catalog of Malin & Carter (1983) shows that about 17% of elliptical galaxies are surrounded by shells. Furthermore, the CCD study of fine structure of E/S0 galaxies (Seitzer & Schweizer 1990) suggests that a significantly higher fraction, about 50%, exhibit these features.

On the theoretical side, more or less systematic efforts have been made to understand the origins and the formation mechanisms of shell structures mainly using numerical simulations (Prieur 1990 and references therein). These simulations show that the shell structure is a purely stellar dynamical phenomenon and can be formed by the phase wrapping or spatial wrapping of the tidally stretched material of a much smaller companion galaxy.

Though the previous numerical studies seem to be successful in explaining shells, some shell galaxies exhibit another peculiarity still to be investigated. Carter et al. (1988) found that 15–20 of 100 shell galaxies of Malin & Carter's (1983) catalog possess peculiar nuclei, the spectra of which suggest dominance of A-type stars. The usual interpretation is that these nuclei are in the poststarburst phase several times 10^8 years after the peak star formation activity (caused during the accretion of the companion galaxy), in which OB stars have already died out, leaving only stars with spectral types later than A. Theoretical studies involving the interstellar gas and the star-formation process are required to clarify the occurrence of possible starbursts and their relationship to the dynamical processes. Hernquist & Weil (1992) and Weil & Hernquist (1993) studied the fate of the interstellar gas originally contained in the companion galaxy in shell formation using the smoothed particle hydrodynamics (SPH) code. Their model shows quick segregation of the gas from the stellar component and efficient gas infall to the center of the elliptical. Though their model does not include the star formation process, they argue that a strong starburst in the center of the elliptical is likely. In this paper we propose a different interpretation on the basis of a series of simulations that include the star formation process explicitly. Dependence of the global gas dynamics on the adopted interstellar gas model is emphasized.

Section 2 describes the numerical methods and the models. Results are presented in § 3. Discussion is given in § 4, and § 5 summarizes conclusions.

2. NUMERICAL METHODS

We consider the sinking of a small spiral galaxy into a giant elliptical galaxy. In the present paper the words "sinking," "accretion," and "merger" are used interchangeably as far as no confusion occurs. Also, the spiral galaxy is called the "satellite" or the "companion." Prior to carrying out a sinking simulation, we must set up equilibrium models of both the elliptical and spiral galaxies. After this, these two galaxies are made to collide with some suitable orbital parameters and spatial configurations. The procedure is described below.

2.1. *Global Structures of the Galaxy Models*

This subsection describes the procedure of setting up equilibrium models that are meant to represent galaxies in an isolated state.

The initial density distribution of the elliptical galaxy is assumed to be spherical for simplicity and to obey de Vaucouleurs' law ($r^{1/4}$ law) with an effective radius r_e. N_E stellar (i.e., collisionless) particles are distributed spherically following this law. $N_E = 19{,}985$ in most cases. Isotropic random motions are given to each particle initially. The

velocity dispersion is calculated in the same manner as that in Hernquist (1993). Before doing a sinking simulation, this model is evolved in isolation for 15.6 time units to ascertain its stability. Here, the time unit is taken to be $(r_e^3/GM_E)^{1/2}$, where M_E is the total mass of the elliptical galaxy and G the gravitational constant. Structural and kinematical properties at the end of this calculation are given in Figure 1. The state indicated in Figure 1 is used as the initial condition of the elliptical galaxy in sinking simulations.

The companion galaxy is a disk galaxy that consists of a halo, a stellar disk, and a gaseous disk. Here, the halo is meant to represent not the entire (dark) halo that might surround the visible galaxy but the portion of the dark halo inside the optical radius and any luminous spheroidal components such as a bulge. The masses of the halo, the stellar disk, and the gaseous disk are denoted by M_H, M_S, and M_G, respectively. All the three components are truncated at the galactocentric radius $r = r_t$. The model is fundamentally based on the model of Fall & Efstathiou (1980). The stellar and gaseous disks both have exponential surface density distributions with the same scale length α. The disks rotate nearly rigidly in the inner parts and at a nearly constant velocity in the outer parts. The turnover radius that divides these two parts is denoted by r_m. The halo and the stellar disk are constructed by N_H and N_S stellar particles, respectively, whereas the gaseous disk is composed of N_G cloud particles. The cloud particles suffer from mutual inelastic collisions and experience star formation as described below. The velocity dispersion of the halo is chosen as follows. First, the isotropic velocity dispersion at each radius is calculated so that the condition for "local virial equilibrium" is satisfied everywhere (see Noguchi 1991 for details). A trial simulation showed that such a condition does not lead to virial equilibrium for the entire system. The ratio of the potential energy, W, to the total energy, E, was $W/E = 2.80$ instead of 2 for the exact equilibrium. In order to avoid this, the velocity dispersion was multiplied by a factor of 0.65, which leads to $W/E = 1.75$.

This disk galaxy model is evolved in isolation before the sinking simulations. First, only the halo component is evolved for 15.6 dynamical times with the disk components fixed. After the halo is relaxed, the disks are activated. At this time, the gravitational force acting on each disk particle is calculated, and the circular velocity is given to that particle so that the centrifugal force is balanced with the gravity. At the same time, small random velocities are given to disk particles, which correspond to a specified Q parameter of Toomre (1964). This state just after the activation of the disks is adopted as the initial condition for the disk galaxy in the sinking simulations.

In the following, we use units so that $M_D = r_t = G = 1$, where $M_D (= M_H + M_S + M_G)$ is the total mass of the disk galaxy. The total mass, M_E, and the initial outer radius of the elliptical galaxy are set to be 10. The effective radius, r_e, is set to be 1. Length and mass are measured in units of r_t and M_D, respectively. Velocities are measured in units of $v \equiv (GM_D/r_t)^{1/2}$. Time, t, is measured in units of the dynamical time of the disk galaxy, $t_d \equiv r_t/v$. In the present study, the masses of the halo, the stellar disk, and the gaseous disk are $M_H = 0.7$, $M_S = 0.24$, and $M_G = 0.06$, respectively ($N_H = 4974$, $N_S = 10{,}000$, and $N_G = 5000$). The scale length of both disks is $\alpha \sim 0.25$, and the turnover radius before halo relaxation is $r_m \sim 0.1$. Toomre's Q parameter was set to be 1.5 for both the stellar and the gaseous disks, meaning much smaller velocity dispersions for the gas disk. Both the stellar and the gaseous disks have a Gaussian density distribution along the z-direction, the dispersions of which are 0.05 and 0.025, respectively. Initial conditions of the companion model are shown in Figure 2.

The sizes and masses of the elliptical and disk galaxy models adopted here roughly satisfy the observed scaling relation for elliptical and spiral galaxies. Suppose that the

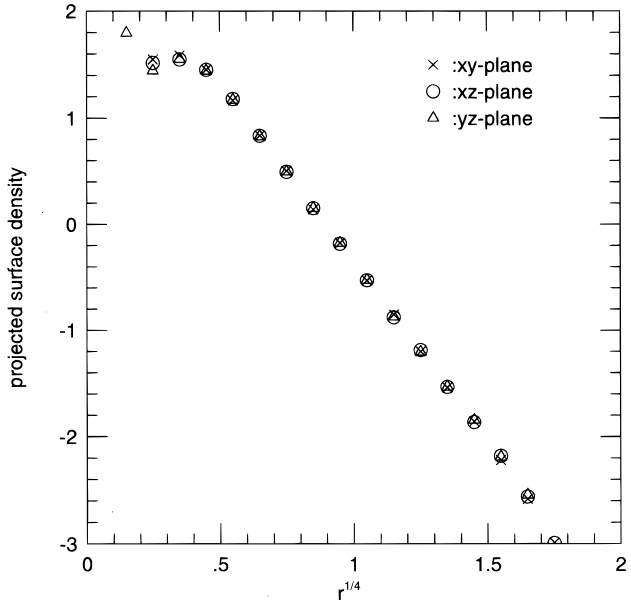

FIG. 1a

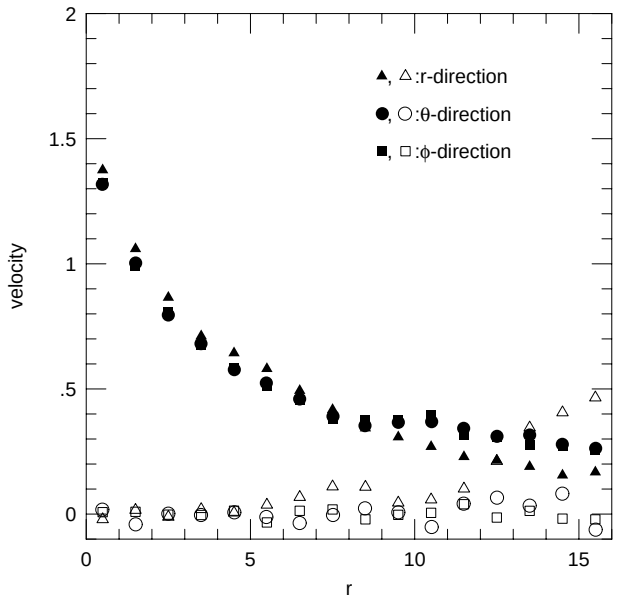

FIG. 1b

FIG. 1.—Elliptical galaxy model. All quantities are given in the unit system in which the total mass and the effective radius of the galaxy are unit mass and length, respectively. The gravitational constant is unity. (*a*) Three surface density profiles projected onto the x-y, x-z, and y-z planes are shown as a function of $r^{1/4}$, where r is the projected distance from the center of the galaxy. (*b*) The profiles of mean velocities (*open symbols*) and velocity dispersions (*filled symbols*). Components along the three directions (r, θ, ϕ) in the spherical coordinate are shown as a function of the radial distance, r, from the center.

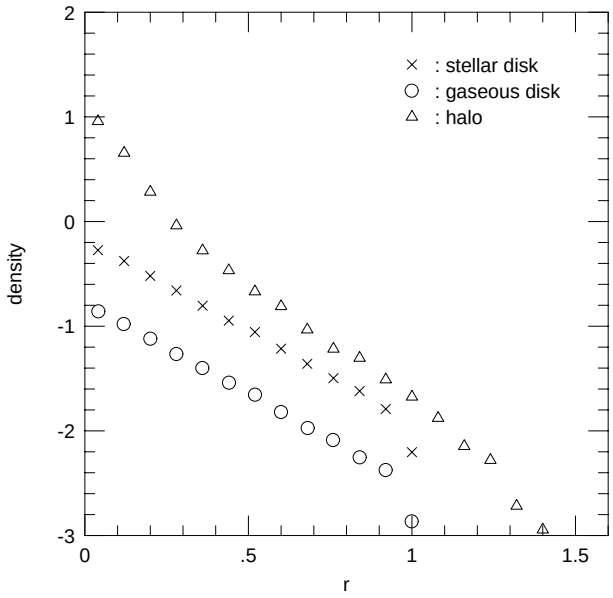

FIG. 2a

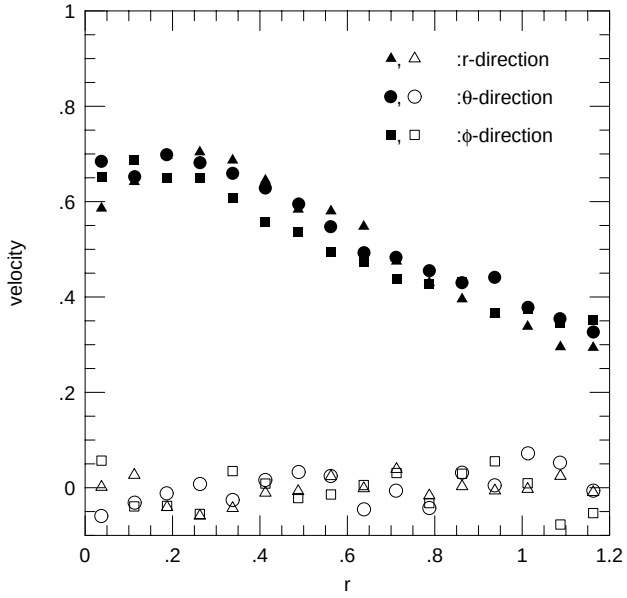

FIG. 2b

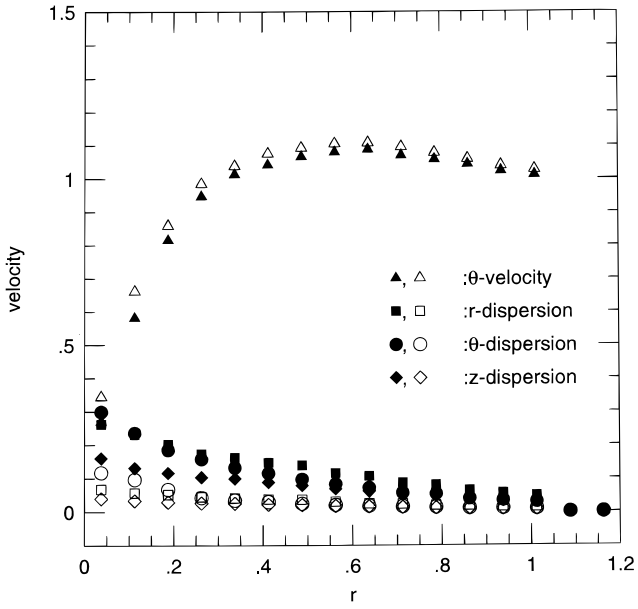

FIG. 2c

FIG. 2.—Satellite disk galaxy model. All quantities are given in nondimensional units described in the text. (*a*) Surface density distributions in the stellar and gaseous disk components and volume density distribution in the halo component derived assuming spherical symmetry for the halo are plotted. The abscissa is the cylindrical radius for the disks and the radial distance from the center for the halo. (*b*) Mean velocities (*open symbols*) and velocity dispersions (*filled symbols*) of the halo in the spherical coordinate system are given as a function of the radial distance, *r*, from the center. The halo was assumed to be exactly spherical in making these plots. (*c*) Tangential (i.e., rotational) velocities (*triangles*) and velocity dispersions in the cylindrical coordinate system (*squares*: radial, *circles*: tangential, *diamonds*: vertical) in the stellar (*filled symbols*) and gaseous (*open symbols*) disks are plotted against *r*, the distance from the center.

disk galaxy model represents a late-type (i.e., Sc) spiral galaxy of an absolute B magnitude $M_B = -20$. Then the isophotal radius [i.e., the radius corresponding to the surface brightness of 25th magnitude (arcsec)$^{-2}$] is typically 10 kpc (see Rubin 1983). This means that the present elliptical galaxy model should have an effective radius $r_e = 10$ kpc. The observed relation between B magnitude and the effective radius (see Kormendy 1977) indicates that the effective radius of this size is typically possessed by an elliptical galaxy with $M_B = -21.5$. Then the question is whether an elliptical galaxy with $M_B = -21.5$ has a mass 10 times large as that of a spiral galaxy with $M_B = -20$, in agreement with the mass ratio adopted in the present simulations. Because the B-band luminosity of the elliptical is nearly 4 times that of the spiral in this case, a 10 times difference in mass is realized if the mass-to-luminosity ratio (in the B band) of the elliptical is 2.5 times that of the spiral. The B-band mass-to-luminosity ratio (m/L_B) for Sc galaxies is around 2.6 (see Rubin 1983). The mass of an elliptical galaxy is generally difficult to determine. The mass calculated by King's method (Richstone & Tremaine 1986) suggests a systematic decrease in the V-band mass-to-

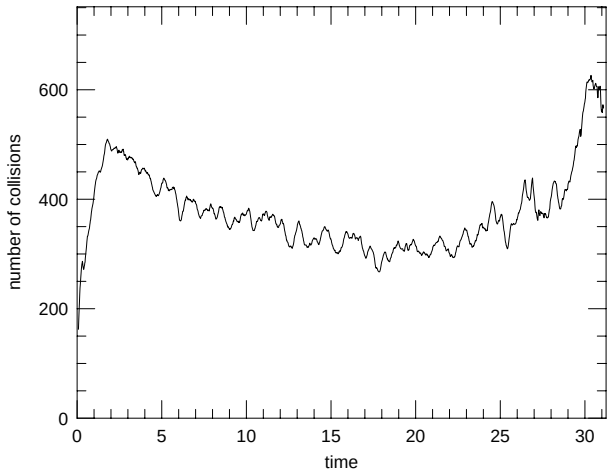

FIG. 3*a*

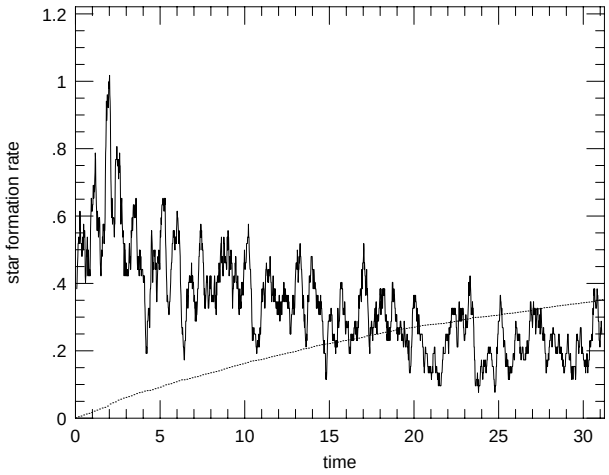

FIG. 3*b*

FIG. 3.—Evolution of the isolated disk galaxy model. (*a*) Number of mutual collisions between gas cloud particles per time step is plotted against time. (*b*) Star formation rate (*solid line*) and the fraction of the gas turned into stars (*dotted line*) are plotted against time. If scaled to a typical Sc galaxy with an absolute blue magnitude of -20, the unit time becomes $\sim 7 \times 10^7$ yr, and the unit star formation rate corresponds to $\sim 1 M_\odot$ yr^{-1}. The same ordinate as for the star formation rate applies to the fraction, and the unity means complete consumption of the gas due to star formation.

luminosity ratio (m/L_V) as M_B increases (Kormendy 1987), giving $m/L_V \sim 6$ for $M_B = -21.5$. There is a color-magnitude relation (see Sandage & Visvanathan 1978) such that a more luminous elliptical galaxy generally has a larger color index $B-V$. However, the gradient of the correlation is very small, and we take $B-V = 0.5$ for the present purpose. This color gives $m/L_B \sim 1.58 m/L_V \sim 9$ for $M_B = -21.5$. Therefore, m/L_B for an elliptical with $M_B = -21.5$ is larger than that of a spiral with $M_B = -20$ by a factor of 9/2.6, or ~ 3.5. Considering the ambiguity involved, this ratio is in agreement with the factor of 2.5 required. This discussion shows that the elliptical and disk galaxy models adopted here have relative masses and sizes consistent with observations.

In the present simulation, the gravitational forces between all the particles are calculated by the TREE code (see Barnes & Hut 1986; Hernquist 1987). The tolerance parameter, θ, which determines the opening angle in constructing a tree structure, is set to be 0.8. The softening length (ϵ) differs depending on the type of particles. The elliptical particles have $\epsilon = 0.04$ in most simulations. The halo particles have $\epsilon = 0.04$, whereas the gas cloud particles and the stellar disk particles have $\epsilon = 0.02$. The softening length of a node in the tree structure is taken to be equal to the mass-weighted mean of individual softening lengths of all the particles and subnodes contained in that node. Particle coordinates and velocities are integrated using the leap-frog algorithm. A fixed time step $dt = 1/64$ is always employed. If scaled to a late-type spiral galaxy with M_B of approximately -20 as above, $M_D \sim 4 \times 10^{10} M_\odot$, $r_t \sim 10$ kpc, $v \sim 130$ km s^{-1}, and $t_d \sim 7 \times 10^7$ yr.

TABLE 1

PARAMETERS OF THE MERGER MODELS

Run	M_E	$V_D(V_x, V_y)$	Comments
1	10.0	(-1.86,[a] 0.0)	radial
2	10.0	(0.0, -0.8[b])	retrograde
3	10.0	(0.0, 0.8[b])	prograde
1B.....	10.0[c]	(-1.90,[a] 0.0)	radial

[a] Escape velocity.
[b] Half the circular velocity.
[c] The gravitational softening length, ϵ, is 0.2 for elliptical particles.

2.2. *The Gas Cloud Model and the Star Formation Algorithm*

The gas cloud particles in our simulations are considered to correspond to the interstellar molecular clouds. Collisions between clouds are treated by the so-called sticky particle method to model the dissipative nature of the interstellar medium (Levinson & Roberts 1981; Roberts & Hausman 1984; Hausman & Roberts 1984). All the cloud particles have the same radius $r_c = 0.005$ (i.e., about 50 pc in physical scale). This choice of cloud size leads to the volume filling factor of the gas clouds of ~ 0.017 in the initial state. In the simulation, two overlapping clouds are made to collide inelastically, provided that they are approaching each other. After collision, the radial component of the mutual velocity is halved and its sign reversed, while the tangential component is unchanged.

One important feature of the present models is that the star formation process is included explicitly in the numerical code. The star formation process is simulated by changing a cloud particle into a new stellar particle. This conversion is performed with a probability that is related to the local gas density around the cloud particle as follows. The local gas density, ρ, for a given cloud particle is determined by counting the number of the gas clouds residing in the sphere of a radius $r_{\rm dens}(=0.075)$ centered on the cloud in question. Then the probability, p, for star formation for this cloud in the current time step is calculated by

$$p = K_{\rm star}\, dt \rho \ .$$

Here, $K_{\rm star}$ is a coefficient that controls the star formation efficiency. The value of $K_{\rm star}$ was determined empirically so that the star formation rate in the equilibrium companion galaxy is nearly the same as the observed values for typical late-type spiral galaxies (see below). After getting p by the above equation, we create a number ξ in the range (0, 1) using the uniform random number generator. If $\xi < p$, we change that cloud particle into a stellar one. This particle is

treated as a collisionless particle afterward. If $\xi > p$, no such transformation is made. This recipe for star formation, namely, converting a whole cloud into a star with some probability instead of converting some fraction of one cloud at every time step, was taken to avoid an intolerable increase of the number of particles in the model. In order to take into account energy input from stellar winds and supernova explosions, each new star is assumed to give a velocity of $v_{sn}(=0.05)$ to all the cloud particles located within the distance of $r_{sn}(=0.02)$ at $t_{sn}(=0.156)$ after its birth. See Noguchi & Ishibashi (1986) for details.

Figure 3 shows the time evolution of the cloud-cloud collision rate and the star formation rate in the isolated disk galaxy model that started from the initial condition given in Figure 2. The cumulative mass of the gas converted to stars is also given as a function of time. Although both rates show short-period fluctuations and secular changes, the amplitudes of these variations still permit us to regard this model as a practically stationary model. Kennicutt (1983)'s estimate based on H_α emission shows that late-type (Sc) galaxies with M_B about -20 typically have a global star-formation rate of ~ 1–$3\ M_\odot\ \mathrm{yr}^{-1}$. The adopted value of K_{star} produces $\sim 1\ M_\odot\ \mathrm{yr}^{-1}$ when scaled to physical units and is considered to be a reasonable choice in view of relatively large range in the observed star-formation rate.

2.3. *Sinking Parameters*

We have carried our several sinking (i.e., merger) simulations using the two galaxy models described above. The orbital plane (i.e., the plane containing the center of the elliptical galaxy and the companion initial velocity vector) is taken to be the x-y plane. Initially the companion center is located on the x-axis. The respective mass centers of the two galaxies are initially separated by 5 length units. The velocity of the companion relative to the elliptical, V_D, is varied as given in Table 1, where V_x and V_y are the x and y components of the companion velocity, respectively. As seen here, we concentrate on radial and nearly radial mergers and do not deal with more circular cases. Initially, the companion disk is parallel to the orbital plane in all the models. The sense of disk rotation (prograde or retrograde) in each model is indicated in Table 1.

3. RESULTS

The main aim of the present study is to investigate the dynamics of the interstellar gas and the star formation process in relation to the formation of shell structures.

The morphological definition of "shells" is somewhat varied in the literature. Some authors use this term in a very restrictive sense, while others prefer looser usage. For example, Dupraz & Combes (1986) have restricted the terminology "shell" to a sharp circular (or slightly elliptical) arc centered on the galaxy and defined a system of shells to be an ensemble of arcs, which do not cross and are regularly spaced around the galaxy. They concentrated on radial merger simulations that tend to produce a regular shell system defined in this way. In contrast, Hernquist & Quinn (1988) term all sharp structures arising in both radial and nonradial merger simulations as shells. From an observational viewpoint, Prieur (1990) classified shell systems into three types according to their morphology. Type 1 are constituted by the aligned systems such as those modeled by Dupraz & Combes (1986) (e.g., NGC 3923), type 2 by the systems in which the position angles of the shells are randomly distributed around the galaxy (e.g., 0422−476 in Malin & Carter [1983] catalogue), and type 3 by all the remaining objects. Here we define the shell structure as a three-dimensional distribution of particles that looks like a system of multiple arclets that are concentric and detached from each other (i.e., type 1 and type 2 in Prieur's 1990 classification) when seen along a favorable line of sight.

In partial agreement with previous studies, we have found that a radial or retrograde merger can create regular (i.e., type 1 or 2) shell structures. Figures 4 shows the snapshots of the radial model, run 1. The initial velocity of the companion is the same as the escape velocity of a test particle located at the same position as the companion in the elliptical potential (hereafter we refer to this velocity as the escape velocity for simplicity). Disk stars, gas clouds, and new stars created from gas clouds after the start of the simulation are shown separately in Figure 4. As seen in Figure 4, stellar particles that initially constituted the stellar disk of the companion galaxy (i.e., disk stars) start to make a clear shell structure after the first collision with the elliptical galaxy. Each shell propagates outward. A multiple shell system of type 1 is clearly discernible at least for $\sim 9 < t < \sim 19$ in this model, i.e., for more than ~ 1 Gyr in the late phase of the accretion. It is noted that the cloud particles develop a similar structure, although the clarity in the shells is much reduced. There is no significant difference in the global distribution between stellar and gaseous debris of the companion disk. New stars also follow the distributions of these two components. Figure 5 demonstrates this similarity in spatial distributions quantitatively. This figure obviously shows nearly the same radial distribution of debris for the two disk components.

This similarity comes from the fact that the cloud particles behave like the stellar particles after the first collision of the companion with the elliptical center in this model. Figure 6*a* shows the total number of collisions between the gas clouds in this model as a function of time. It is seen that the collisions between the clouds are effectively reduced after the companion has passed the elliptical center. When the companion passes the elliptical center, the gaseous disk is heavily destroyed. The gas clouds are dispersed into a large volume of space, because the central part of the elliptical galaxy acts as an efficient scattering center because of its deep potential well. This scattering leads to decrease in the gas density and, hence, a decrease in the cloud-cloud collision rate. After this the gas clouds become essentially collisionless, mimicking stellar dynamics. This point, i.e., the lack of significant segregation between the stellar and gaseous debris, is in marked contrast with the result by Hernquist & Weil (1992) and Weil & Hernquist (1993), who used SPH description of the interstellar gas and obtained a quick segregation of the gas from the stellar debris. We will discuss this point later.

Figure 7 is the same snapshot as Figure 4 but for the slightly retrograde model, run 2. In this model, the initial velocity is taken to be half the circular velocity, and the velocity vector was directed toward the negative y-direction. In this case, the companion gradually sinks toward the center of the elliptical galaxy. In the later phases (i.e., $t \gtrsim 18$), both the disk stars (Fig. 7*a*) and gas clouds (Fig. 7*b*) show a multiple shell structure that lasts at least for ~ 1 Gyr to $t = 28$, when the simulation was terminated. In this case, the shells are not oppositely placed with respect to the elliptical center as in the radial model, run 1, but randomly

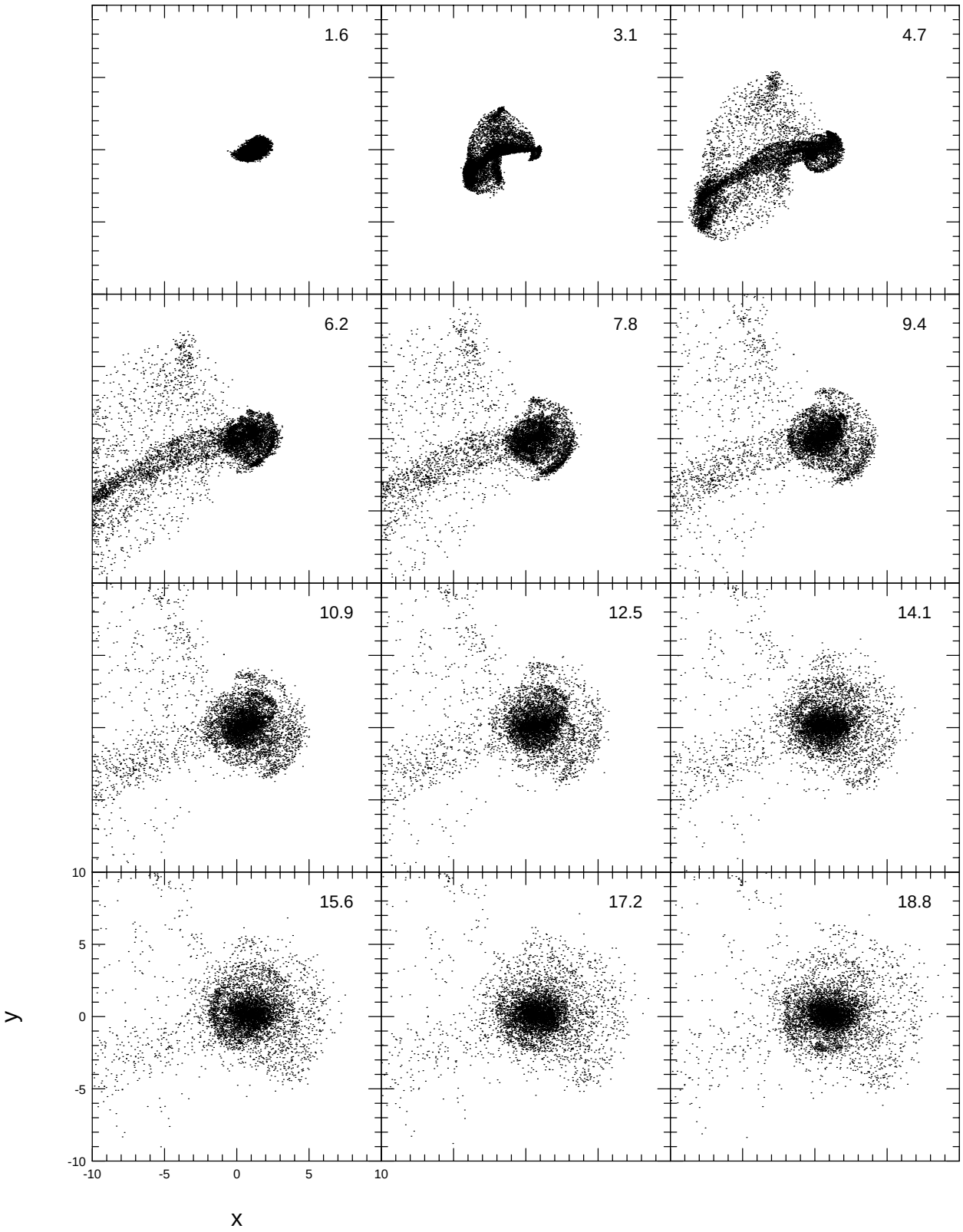

FIG. 4*a*

FIG. 4.—Morphological evolution of the radial merger model, run 1. (*a*) Projection of the disk stars onto the *x*-*y* plane, which is the orbital plane of the satellite galaxy. Time, *t*, is given at the upper-right corner of each frame. Initially (i.e., at $t = 0$), the center of the satellite is located at $x = 5$, $y = 0$ with its disk rotating counterclockwise in the *x*-*y* plane. The satellite is launched into negative *x*-direction with escape velocity. The new stars born from the gas clouds after the start of the simulation are not included in the plot (see panel *e*). (*b*) Same as (*a*), but for projection onto the *x*-*z* plane. Three-dimensional nature of the shells is clearly seen (e.g., $t = 12.5$). (*c*) Same as (*a*), but for the gas cloud particles. Only those clouds are plotted that have not yet experienced star formation at the time indicated. (*d*) Same as (*c*), but for projection onto the *x*-*z* plane. (*e*) Projection of new stars born from gas clouds into *x*-*y* plane. All the new stars existing at the current time are plotted. Large crosses indicate stars having an age less than 0.1 time units (i.e., $\sim 10^7$ yr), whereas stars older than 0.1 but younger than 1 time units (i.e., $\sim 10^8$ yr) are plotted as small crosses. Dots indicate stars older than 1 time unit. A smaller area than in panels (*a*) and (*c*) is displayed for clear representation.

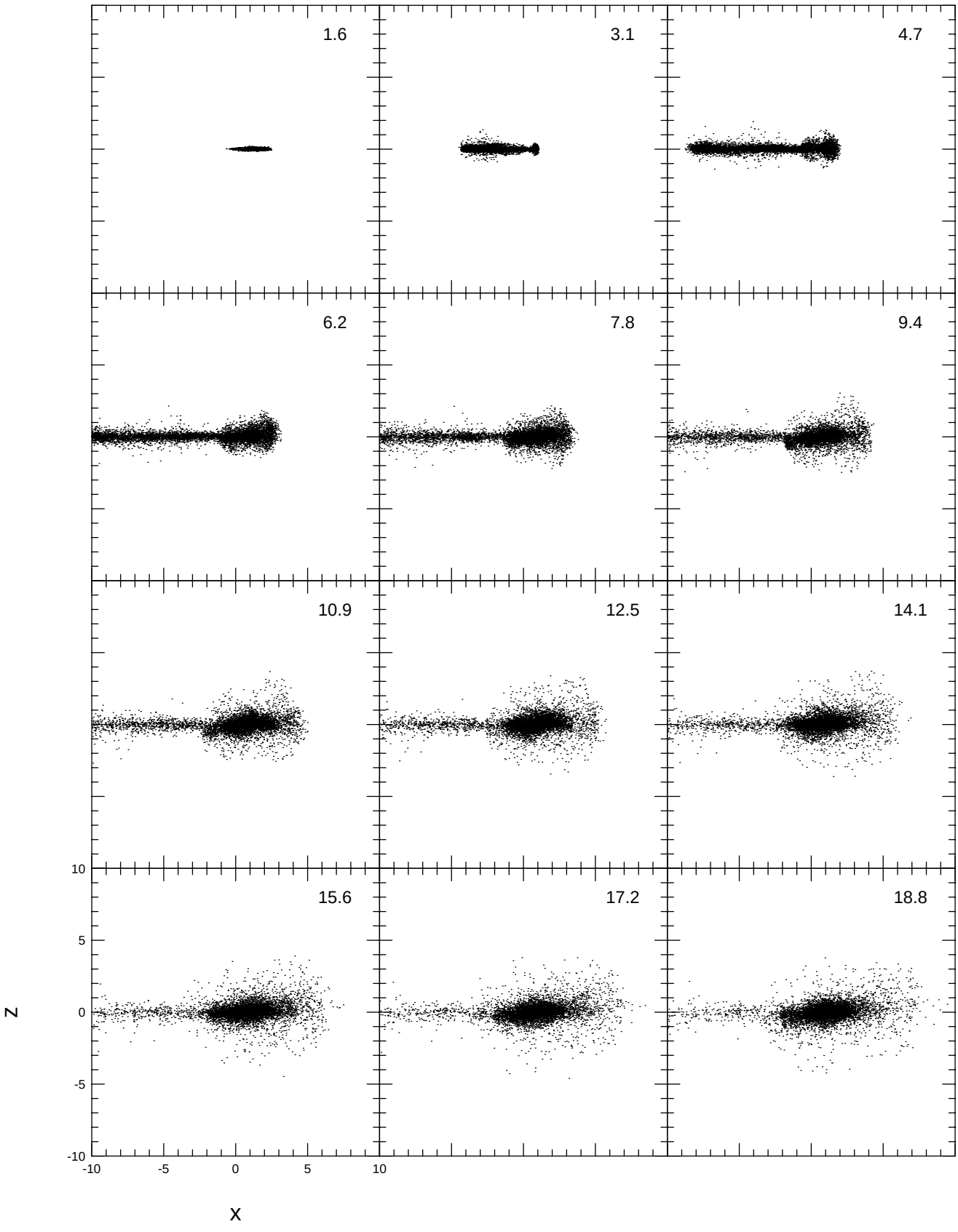

FIG. 4*b*

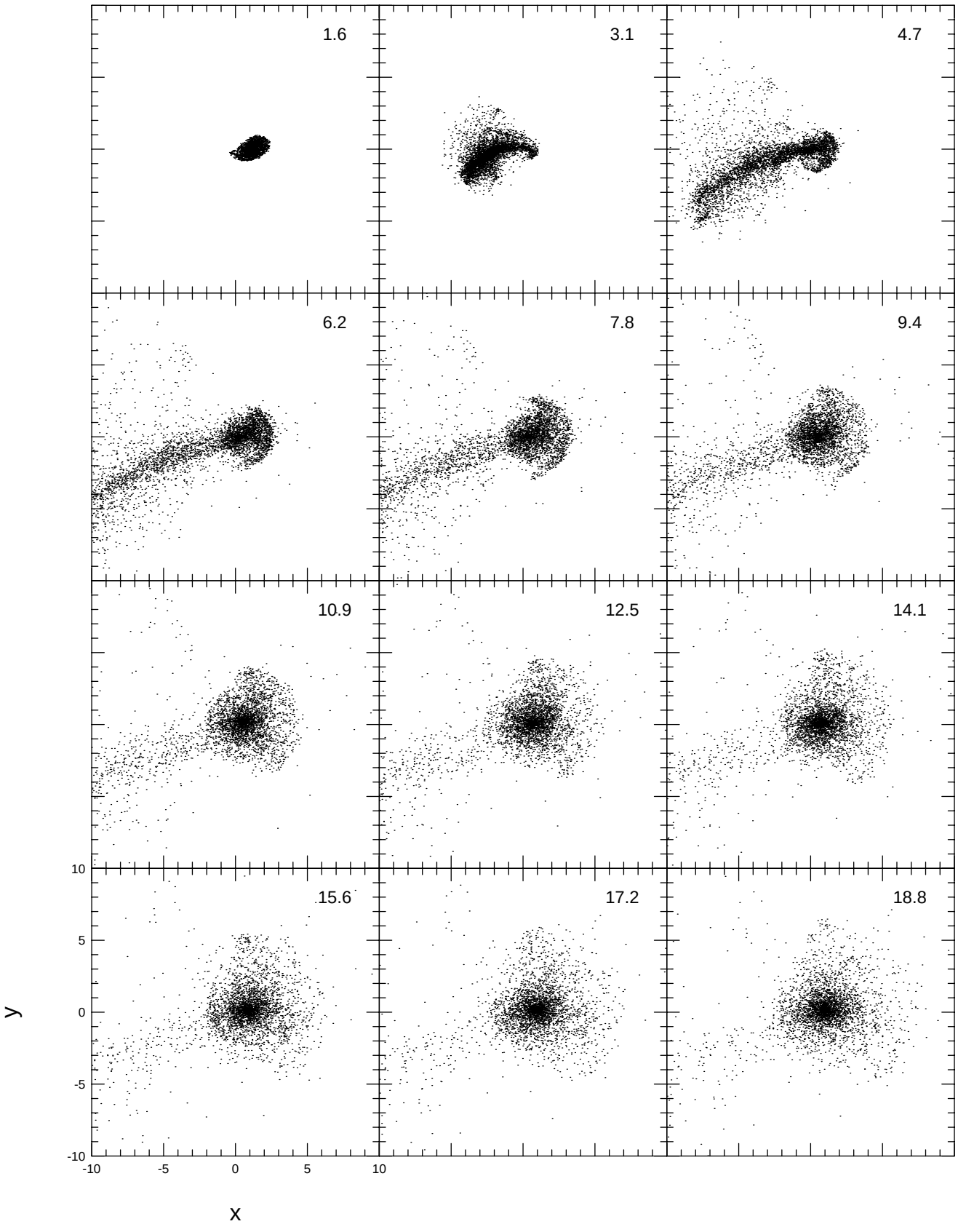

FIG. 4*c*

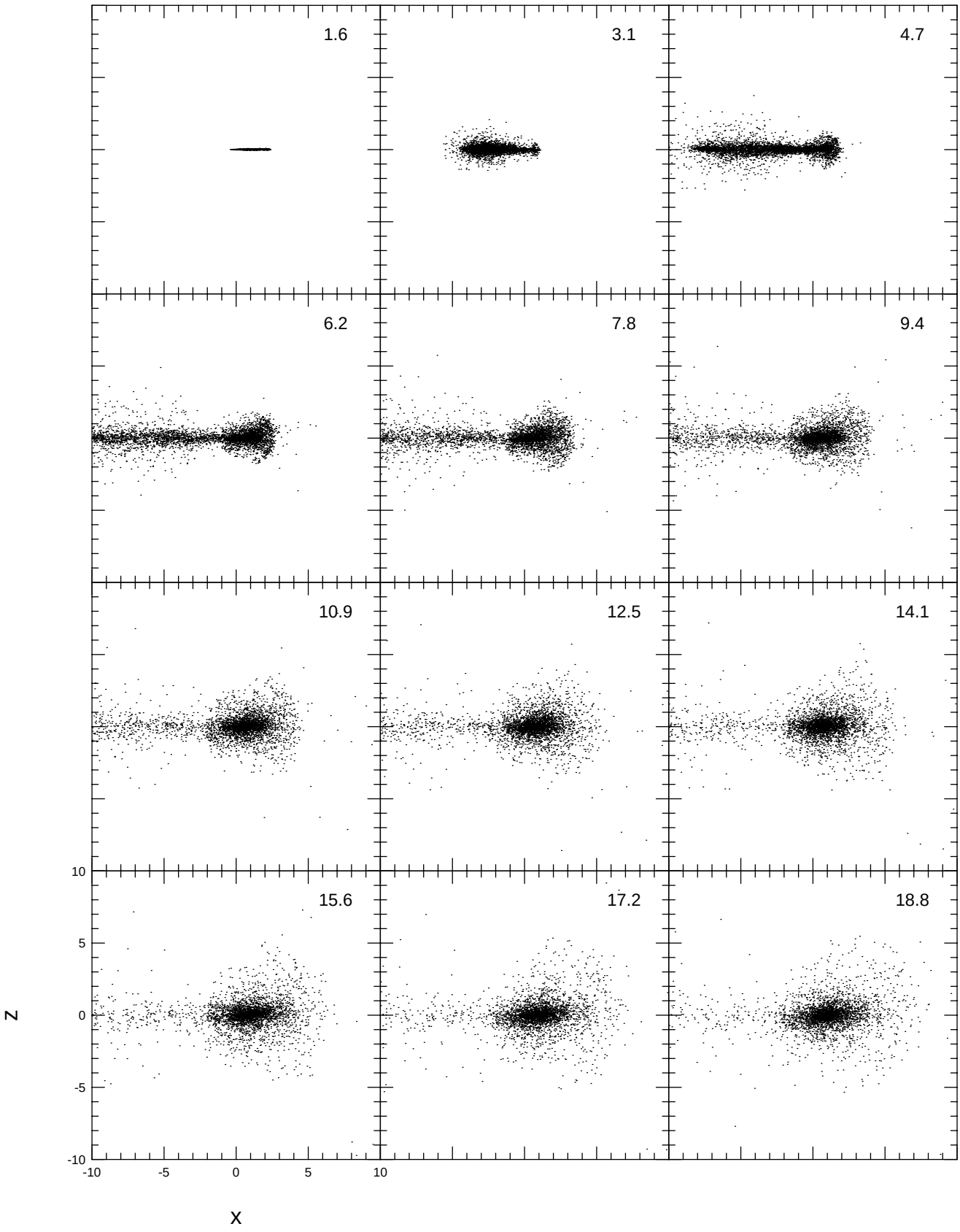

FIG. 4*d*

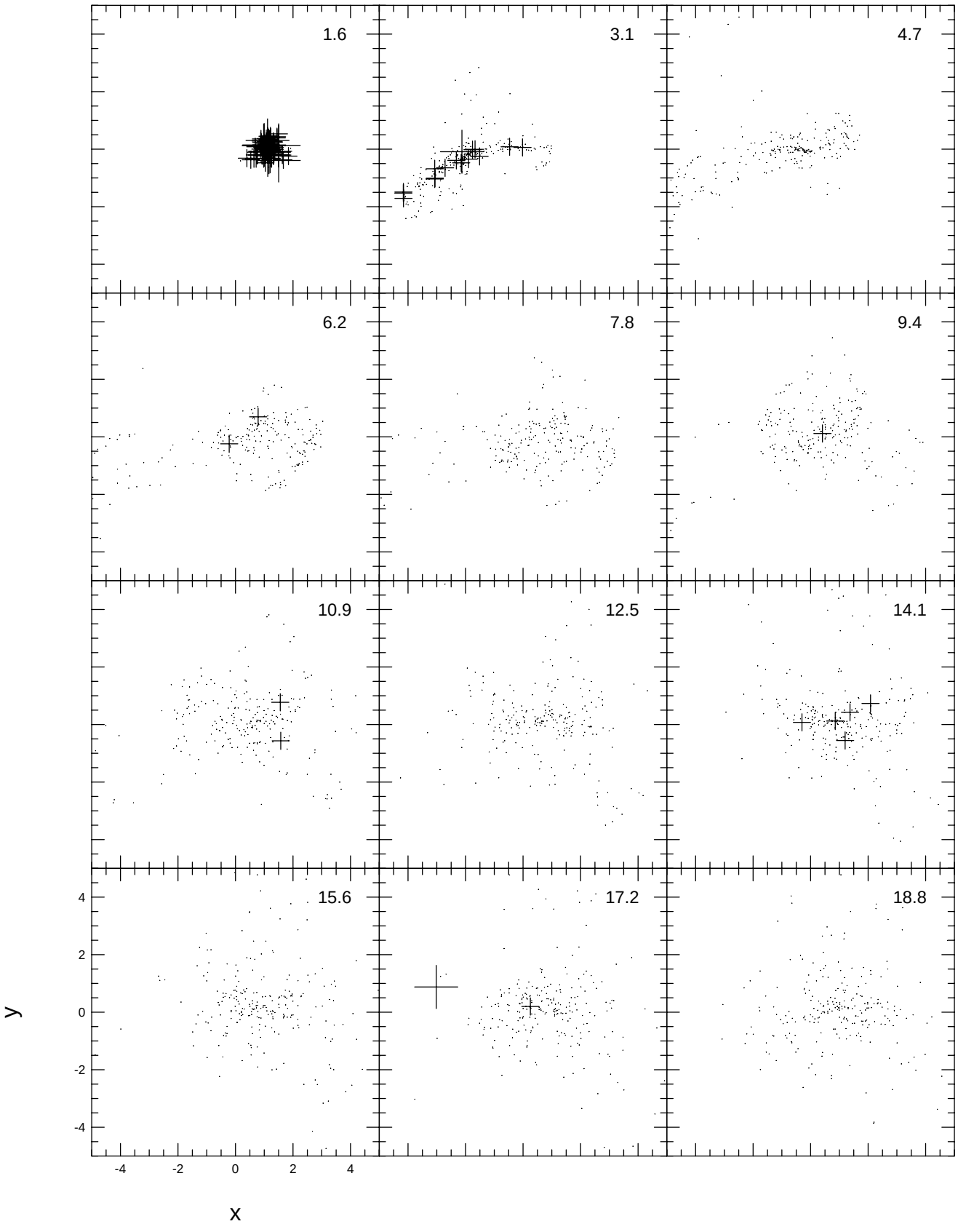

FIG. 4*e*

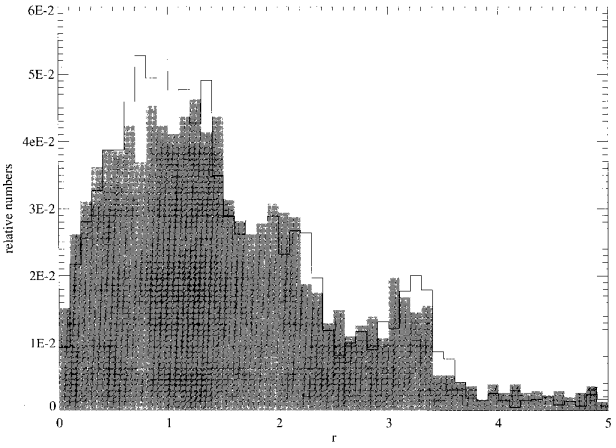

FIG. 5.—Radial distribution of the stellar (*solid line*) and gaseous (*hatched region*) particles around the center of the elliptical at $t = 9.4$ in run 1. Relative numbers are calculated by counting the number of particles included in each radial bin and normalizing them so that the areas of both histograms become the same. The new stars formed from the gas clouds are not included in either histogram.

located around the elliptical center (type 2 in Prieur's [1990] classification). However, this model is similar to run 1 in that the stellar particles and the clouds have the same spatial distribution globally. The new stars also show a similar distribution to these two components, although their paucity in number makes shell structures more difficult to recognize (Fig. 7*c*). Figure 6*b* shows the total collision number of gas clouds as a function of time. In this model, the collision number is increased remarkably in late phases, but this is primarily due to the condensation of clouds in the central part of the companion. At 15.6 time units, the total collision number is 2215 and the number of currently colliding clouds is 333 for the entire cloud system. Of these, 2214 collisions are taking place within 0.05 length units from the density center of the cloud disk in the satellite galaxy. This central region contains 331 colliding clouds. The clouds are widely spread, and the collision number is decreased in the outer parts, where shell structures develop.

Figure 8*a* shows the time variation of the star formation rate in the radial merger model, run 1. It is seen that the star formation rate is abruptly reduced around the time of the first passage of the companion through the center of the elliptical galaxy. A spiky burst is recognized just before this. However, this does not contribute significantly to the amount of star formation because of its very short duration (see the dotted line, which shows the cumulative mass of new stars created from the gas clouds). This abrupt truncation of star formation at the time of collision is due to the sudden decrease in gas density caused by the gravitational scattering by the elliptical potential, which is mentioned before. In the case of the retrograde model run 2 (Fig. 8*b*), we also see a decrease in the star formation rate, but this time it is gradual, in correspondence with the relatively gradual disruption of the gaseous disk. In both run 1 and run 2, star formation has practically ceased several times 10^8 yr before the shell structure becomes evident. Based on this result, we propose that the "poststarburst" nuclei observed in many shell galaxies are not always the result of a starburst but could be the outcome of abrupt truncation of star formation (see § 4).

Prograde models show a qualitatively different evolution from the radial or retrograde ones. In run 3, the initial velocity has the same value as in run 2, the retrograde model, but its direction is contrary to that in run 2. Figure 9 shows that no discenible shell structure is formed in a prograde sinking. As the satellite galaxy approaches the elliptical galaxy, an increasingly large amount of the material is tidally detached from the outer part of the satellite and forms a continuous loop structure encircling the center of the elliptical. However, the inner part of the satellite survives tidal disruption and remains gravitationally bound. Though not evident in Figure 9, a smaller scale plot clearly shows that a small stellar bar is formed in the center of the satellite at $t \sim 7$ and persists until $t \sim 10$. During this period, the gas clouds are gathered toward the nucleus of the satellite galaxy by the gravitational torque of the bar in the same manner as extensively discussed by Noguchi (1988). Figure 8*c* shows the change of the star formation rate in run 3. The strong starburst seen from $t \sim 6$ to $t \sim 12$ takes place near the satellite center, fueled by this bar-driven gas inflow (see Fig. 9*c*). It is noted that, although a strong starburst is triggered in this case, the epoch when the loop system is most developed ($t > 15$) corresponds to a period of very low star formation activity.

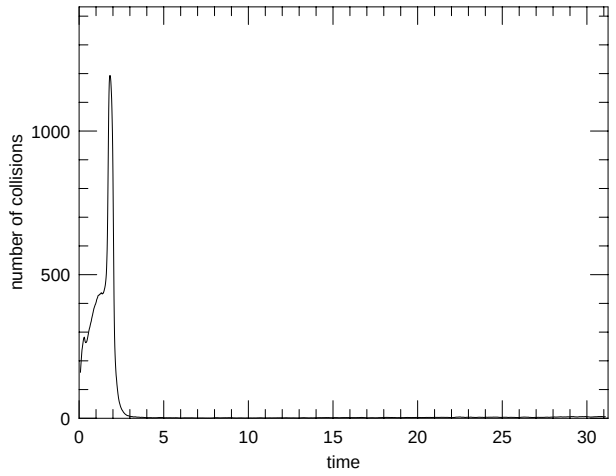

FIG. 6*a*

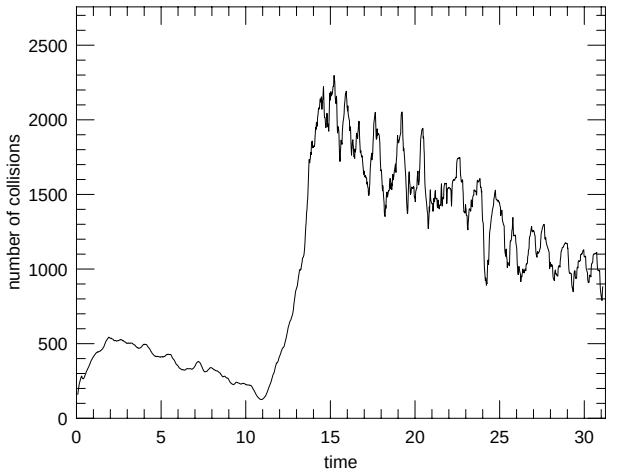

FIG. 6*b*

FIG. 6.—Number of mutual collisions per time step between the gas cloud particles plotted against time for (*a*) the radial model, run 1, and (*b*) the retrograde model, run 2.

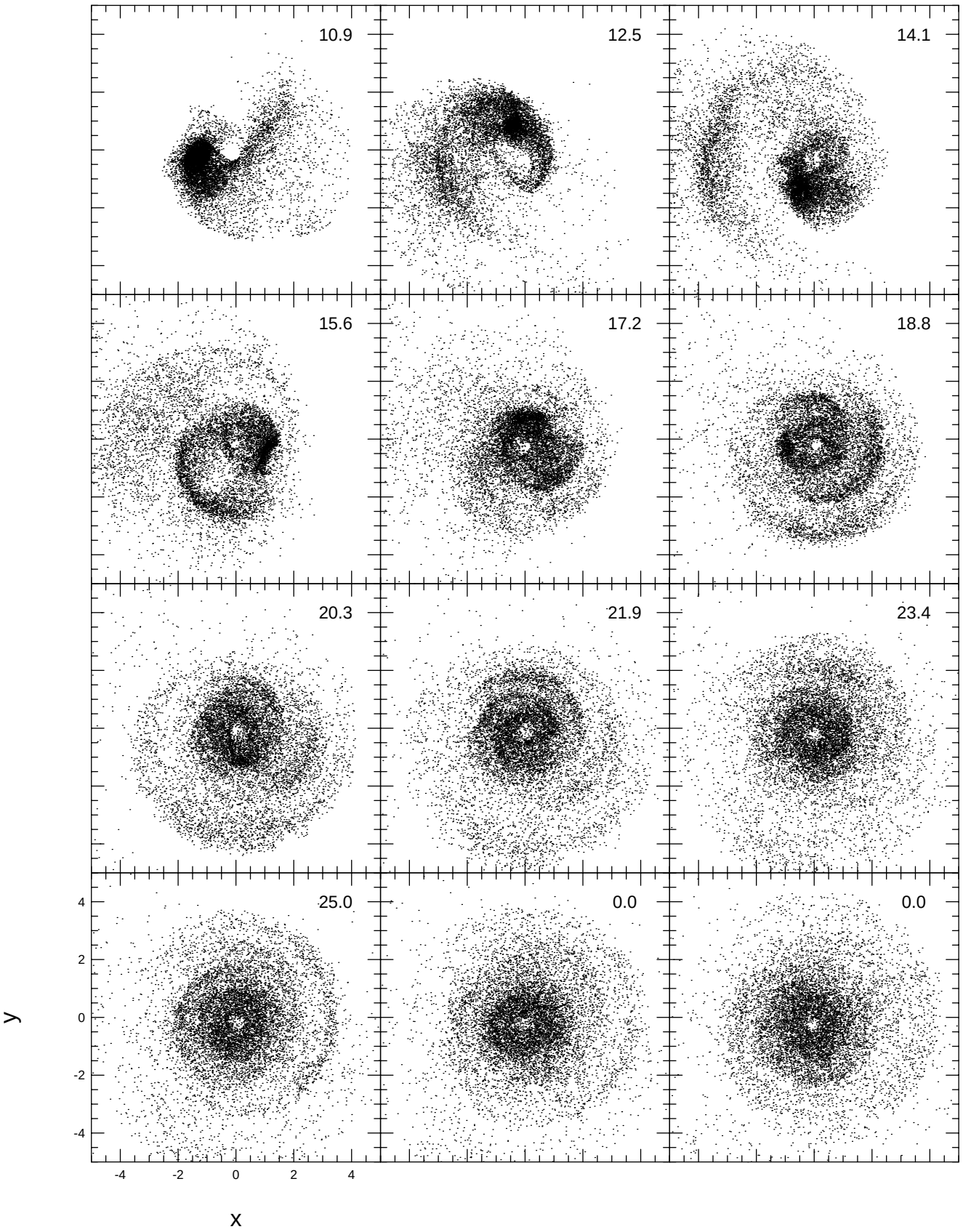

FIG. 7*a*

FIG. 7.—Morphological evolution of the retrograde merger model, run 2. (*a*) Projection of the stellar particles (disk stars) onto the *x*-*y* plane, which is the orbital plane of the satellite galaxy. Time, *t*, is given at the upper-right corner of each frame. Initially (i.e., at $t = 0$), the center of the satellite is located at $x = 5$, $y = 0$ with its disk rotating counterclockwise in the *x*-*y* plane. The satellite is launched into negative *y*-direction. (*b*) Same as (*a*), but for the gas cloud particles. The stars formed from the gas clouds are not included in these plots. (*c*) New stars plotted on the *x*-*y* plane. Symbols have the same meaning as in Fig. 4*e*.

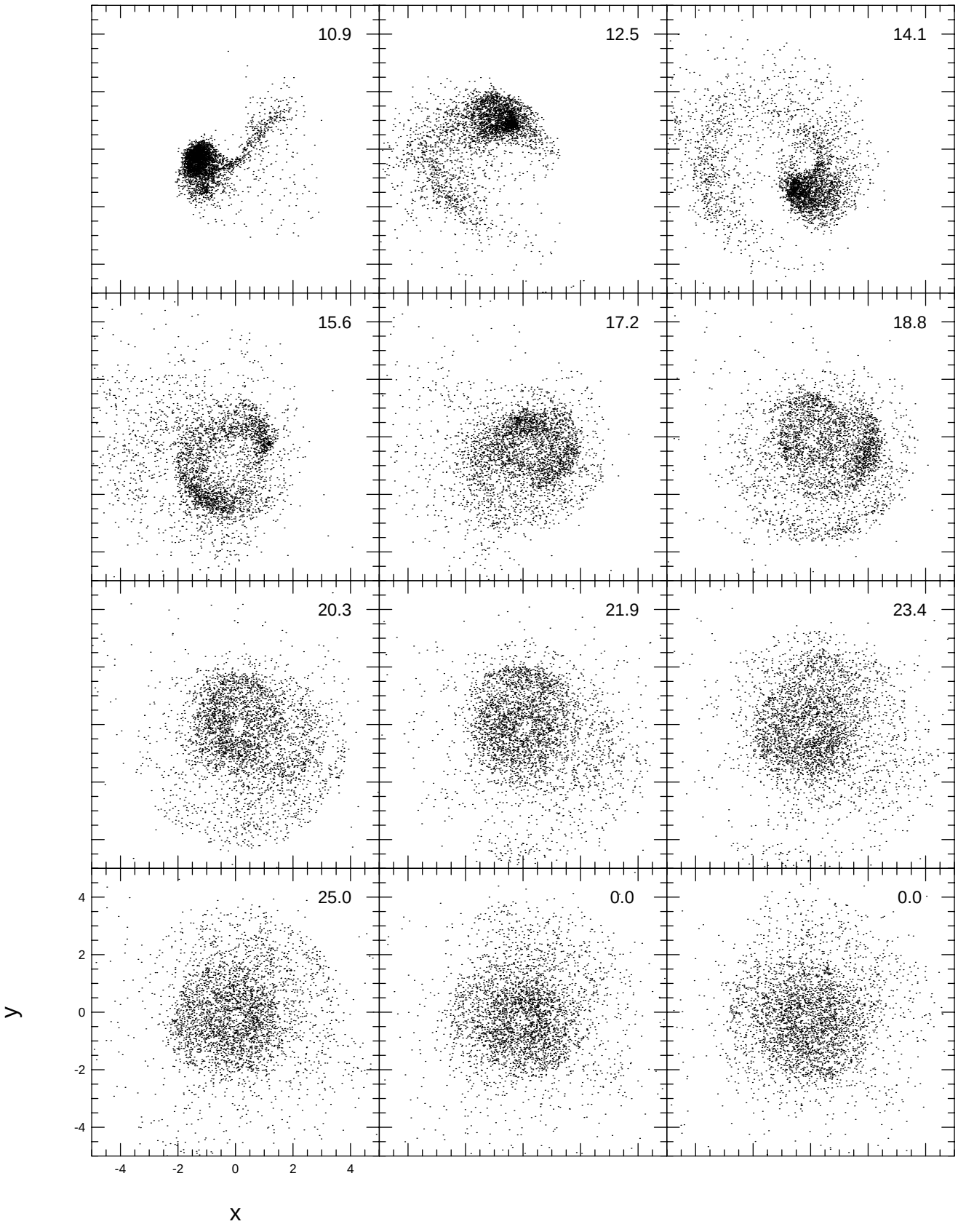

FIG. 7*b*

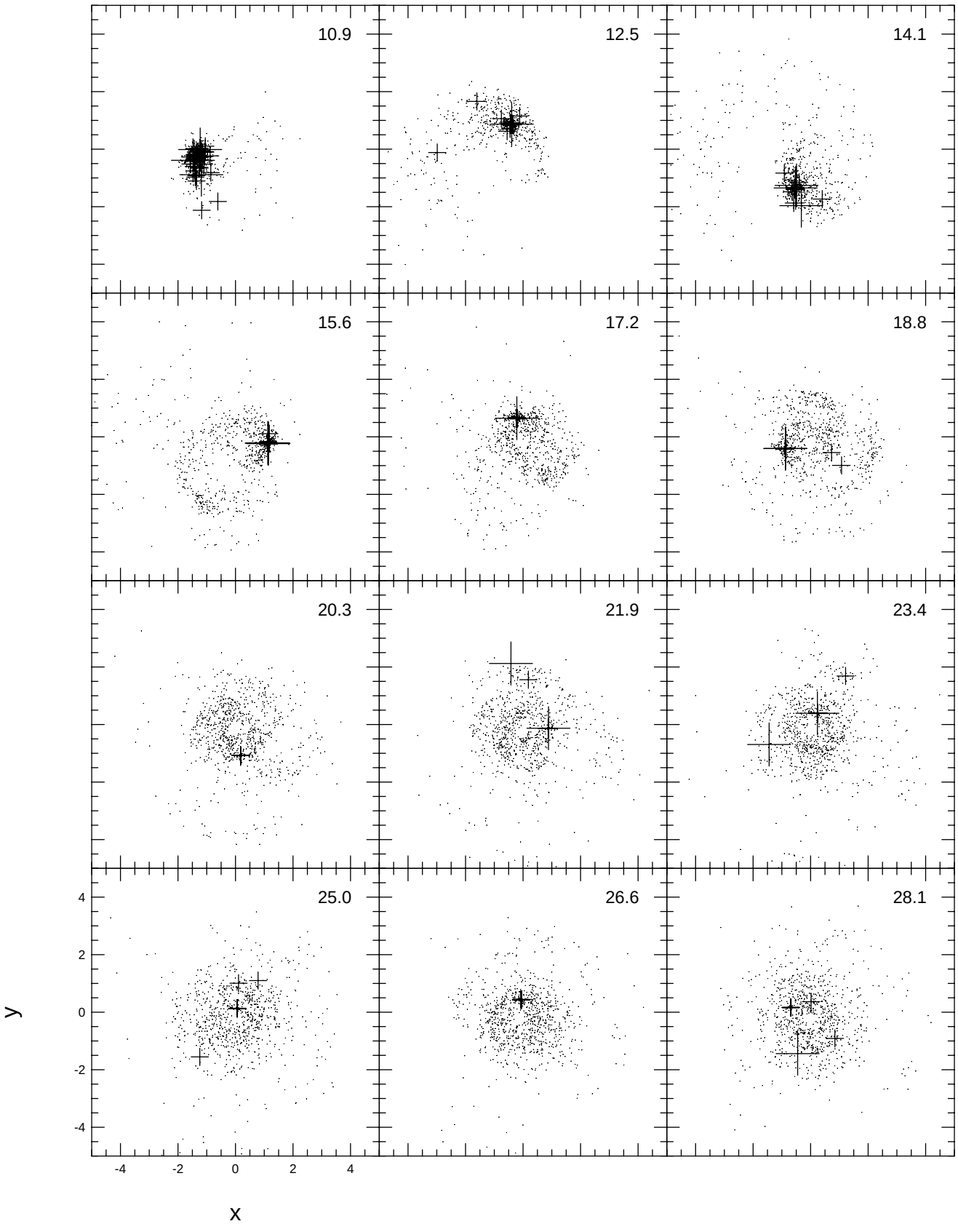

FIG. 7*c*

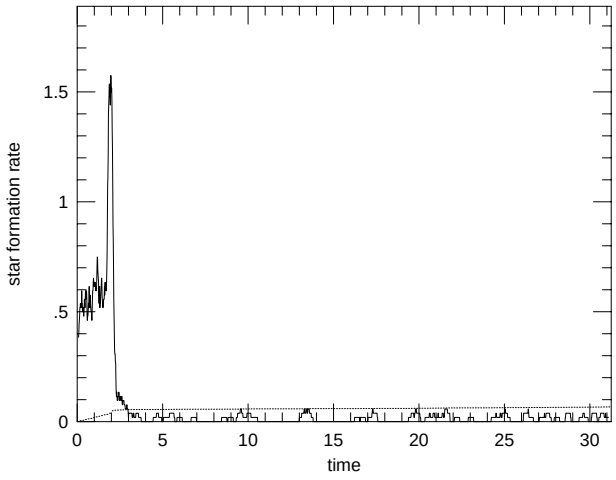

FIG. 8*a*

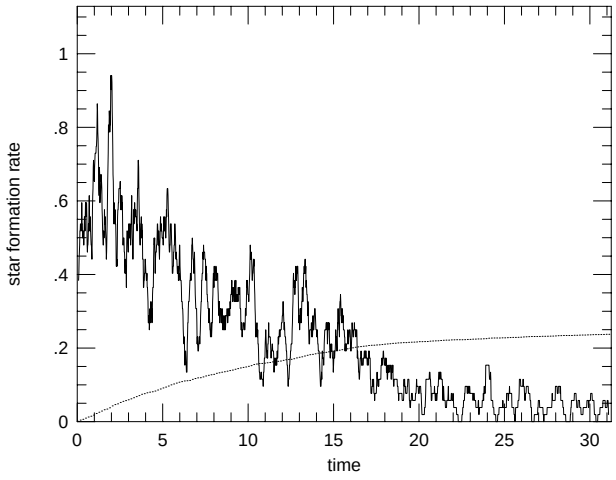

FIG. 8*b*

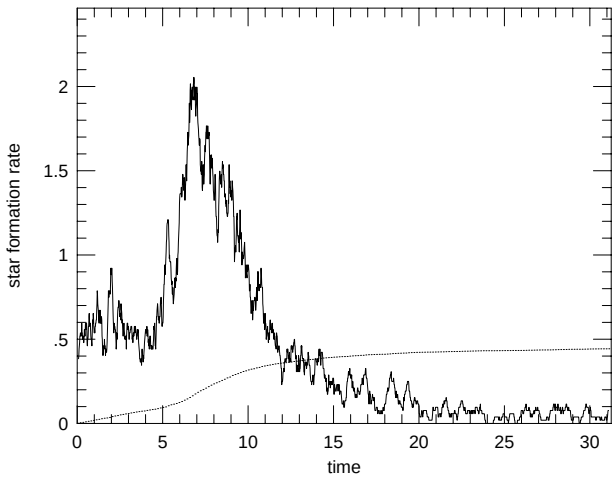

FIG. 8*c*

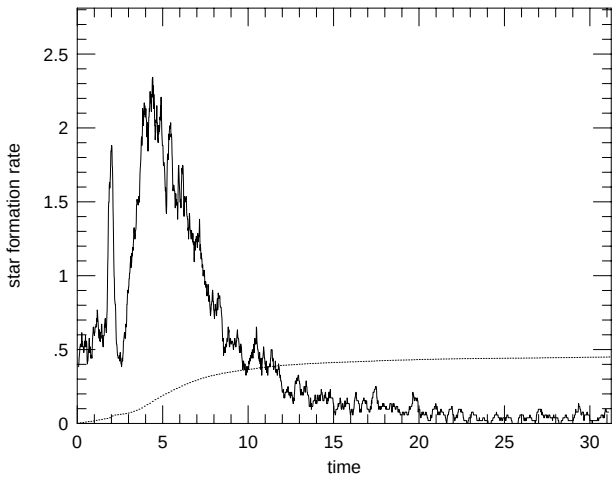

FIG. 8*d*

FIG. 8.—Temporal change in the star formation rate (*solid line*) and the fraction of the gas turned into stars (*dotted line*) for (*a*) the radial model, run 1; (*b*) the retrograde model, run 2; (*c*) the prograde model, run 3; and (*d*) the radial model, run 1B. The ordinate indicates nondimensional star formation rates (in the same unit as in Fig. 3*b*) or nondimensional fractions (i.e., unity means complete consumption of the gas owing to star formation).

Finally we have carried out run 1B to investigate the dependence of the sinking process on the compactness of the elliptical galaxy. This model is the same as the radial model, run 1, except that the central gravitational well of the elliptical is more rounded than that of run 1 owing to the adoption of a larger softening parameter, $\epsilon = 0.2$, for the elliptical particles ($N_E = 9954$ in this model). As Figure 10 indicates, this model tries to make a shell structure as in run 1. In this case, however, the blunt core of the elliptical fails to destroy the companion completely. As the remnant of the companion oscillates back and forth through the central part of the elliptical, it destroys the emerging shells and prevents the formation of a persistent shell system. Temporal change of the star formation rate in this model (Fig. 8*d*) is similar to that in the prograde model, run 3. A strong starburst is triggered ($\sim 3 < t < \sim 8$) because the central part of the companion survives tidal disruption and maintains its identity for a long time. Almost all the star formation takes place in this remnant (see Fig. 10*c*). These results show that the core radius of the elliptical is one of crucial parameters that control the formation of persistent shell structures and the triggering of starbursts.

In summary, we have found that the triggering of starbursts is incompatible with the formation of a regular and persistent shell structure, although in a limited range of parameters. The shell formation requires almost complete disruption of the companion galaxy and scattering of the tidal debris into a large volume, and this process inevitably suppresses star formation. Implications of this result are given in the next section.

4. DISCUSSION

Shell galaxies have a record of extensive researches in the past. Schweizer (1980) was probably the first to suggest that shells would result from a merger (for other ideas, see Fabian, Nulsen, & Stewart 1980; Williams & Christiansen 1985; Wallin & Struck-Marcell 1988; Thomson & Wright 1990). Following this suggestion, many numerical studies have been carried out with various degrees of computational complexity, ranging from test particle simulations (e.g., Quinn 1984; Dupraz & Combes 1986) to completely self-consistent treatments (e.g., Salmon et al. 1990).

Owing to these more-or-less systematic efforts in the past, it appears that we have reached an essentially correct understanding of many aspects of shell galaxies directly related to stellar dynamical processes. The present study is

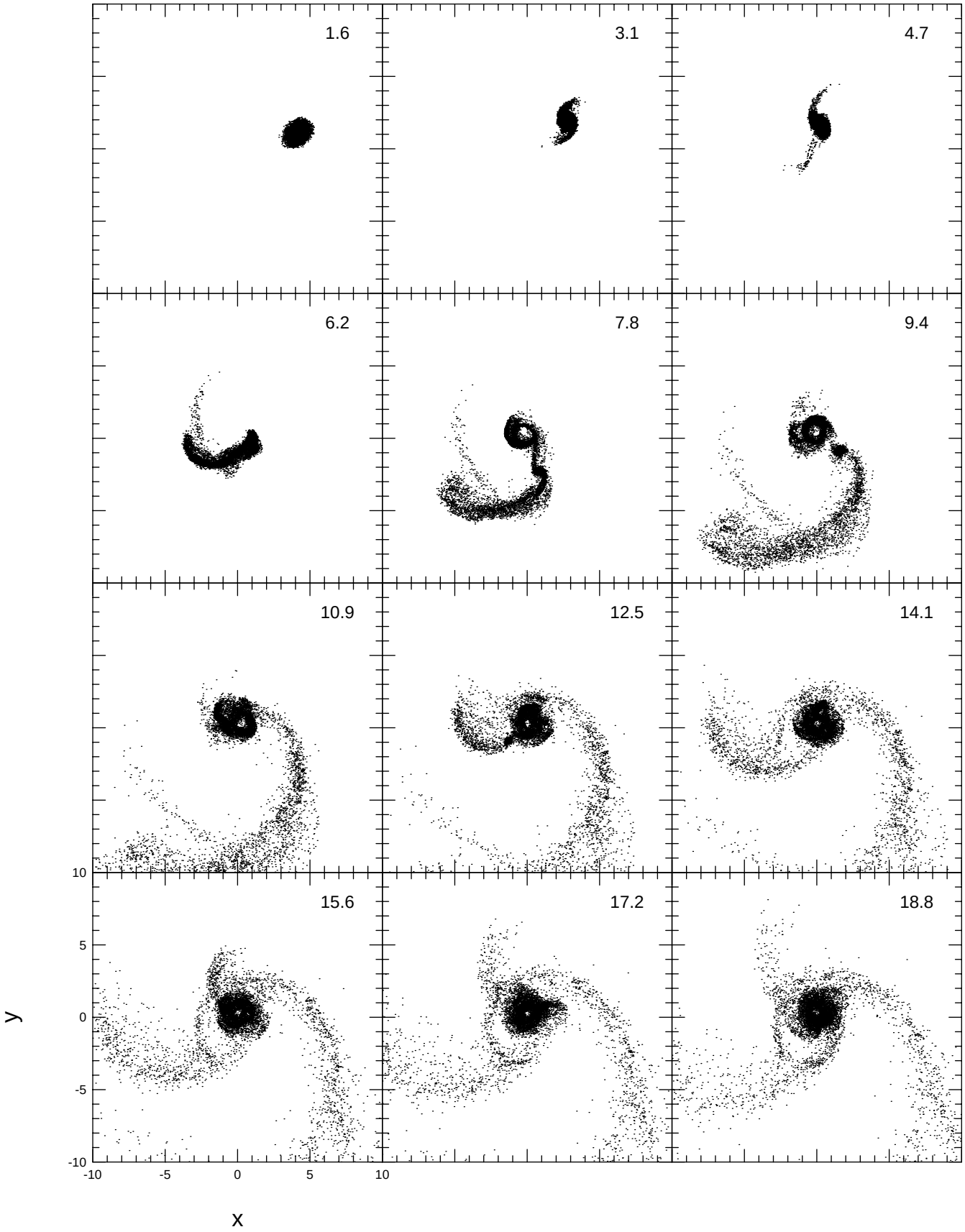

FIG. 9*a*

FIG. 9.—Same as Fig. 7 but for the prograde merger model, run 3. The satellite is launched into positive *y*-direction at $t = 0$. Note the change of scale in panel *c*.

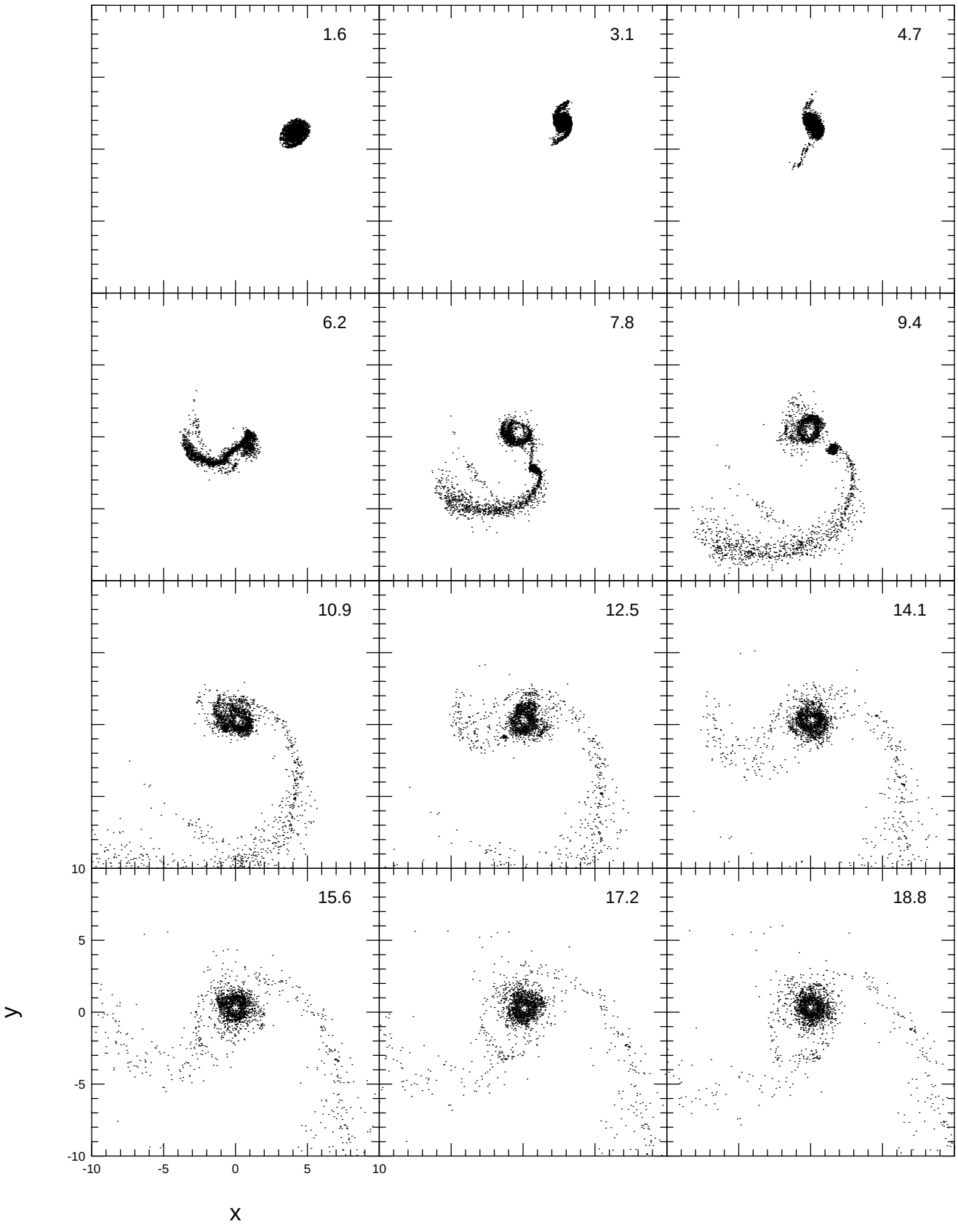

FIG. 9*b*

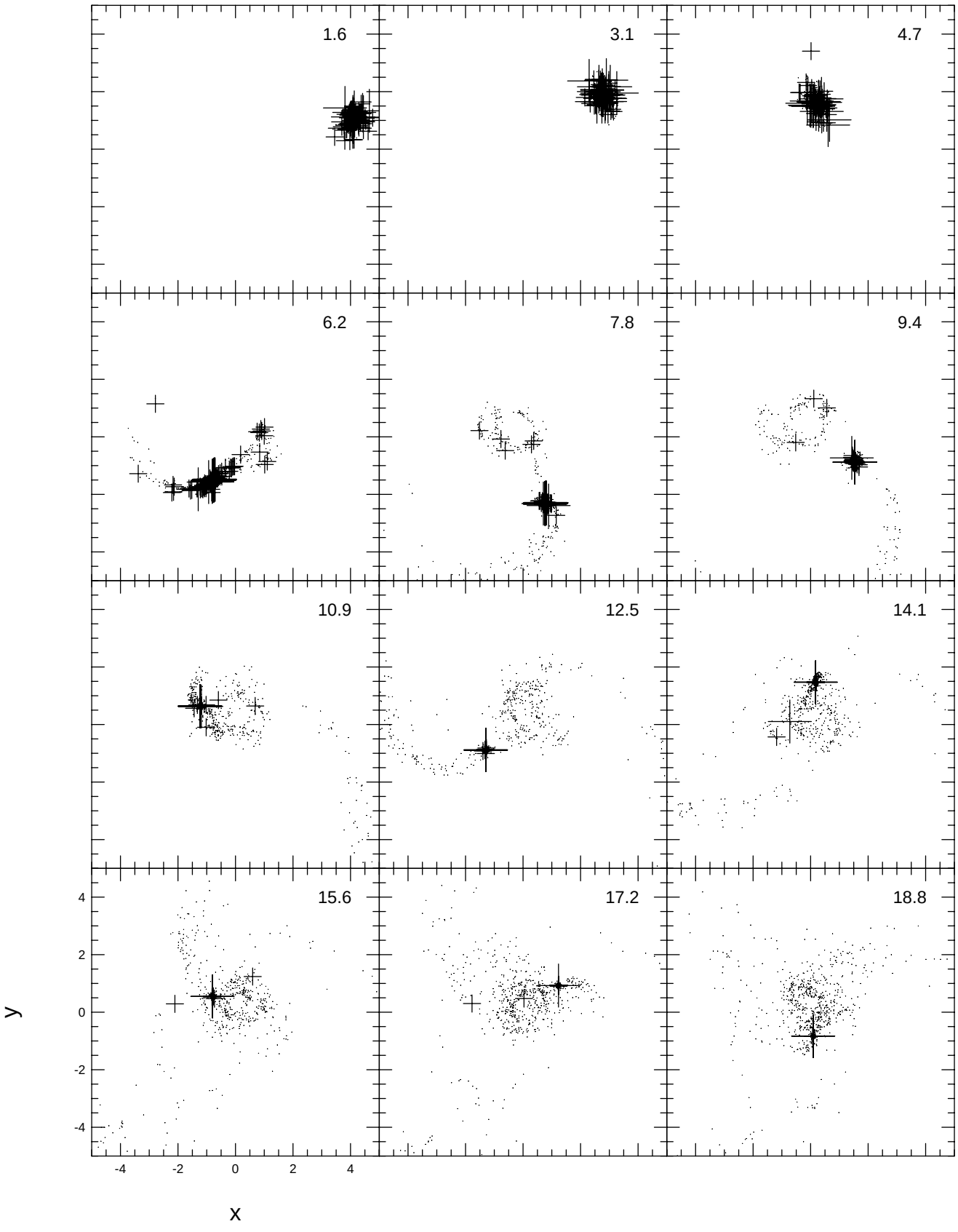

FIG. 9*c*

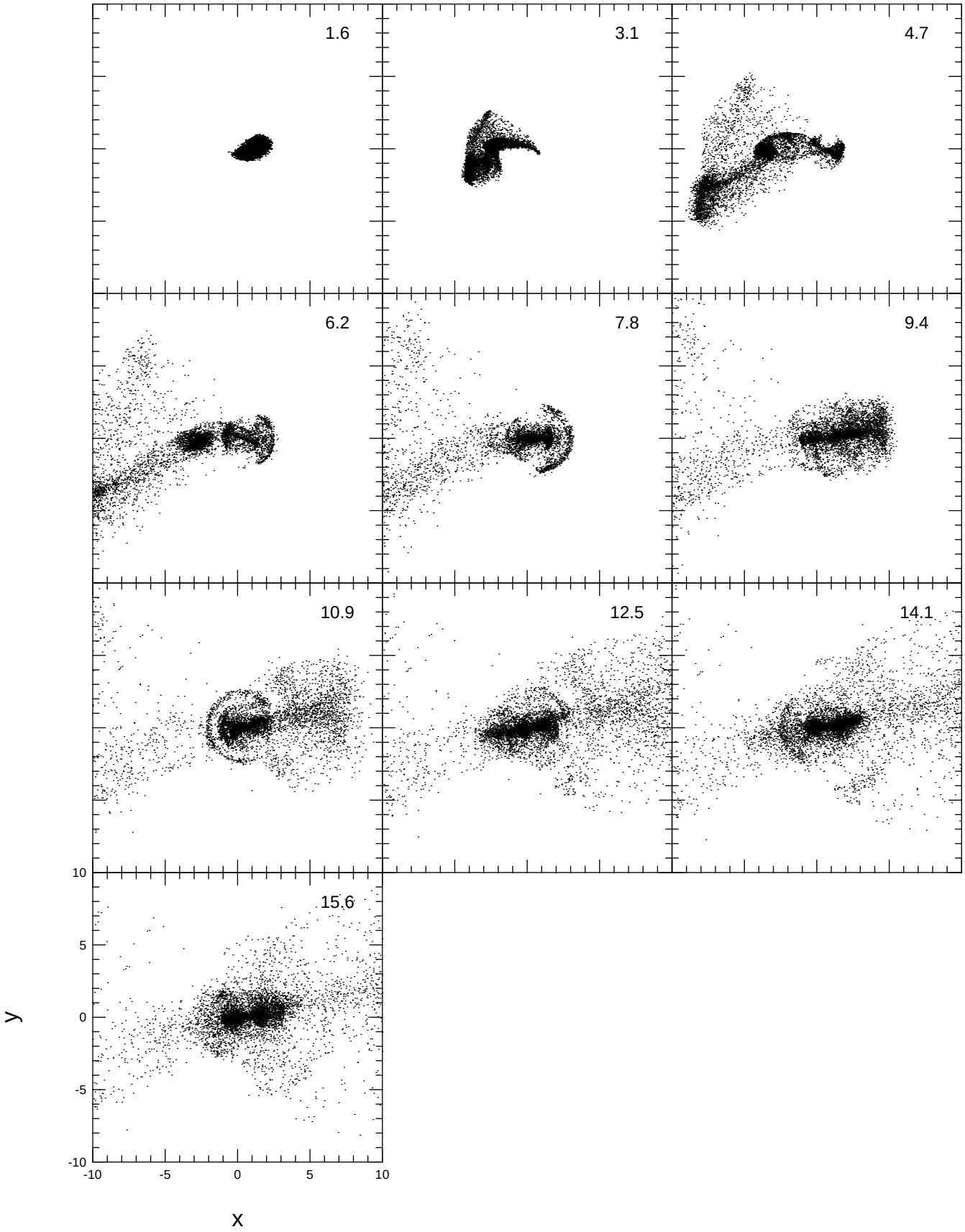

FIG. 10*a*

FIG. 10.—Same as Fig. 7 but for the radial merger with an elliptical galaxy having a blunt core (run 1B). Note the change of scale in panels *b* and *c*.

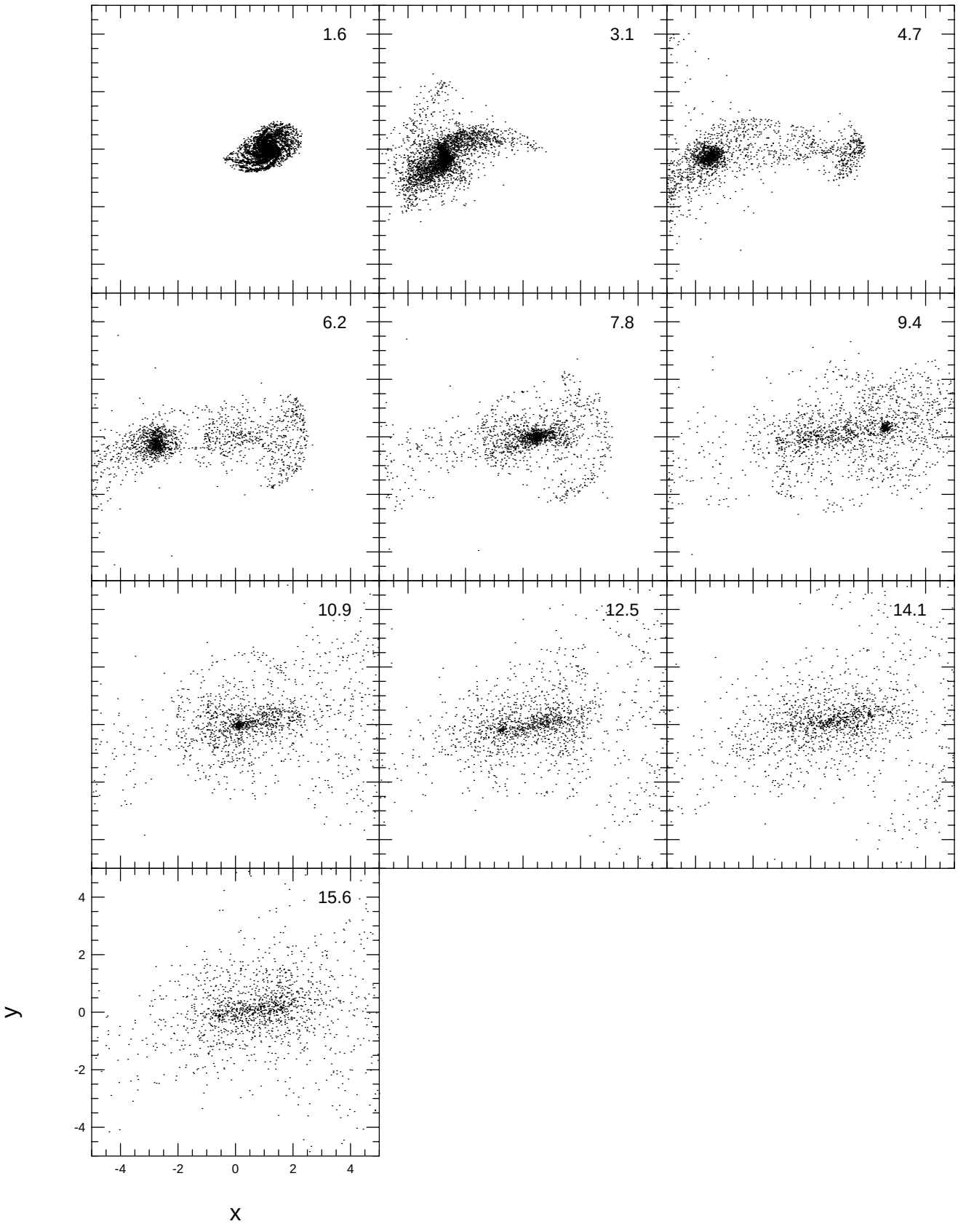

FIG. 10*b*

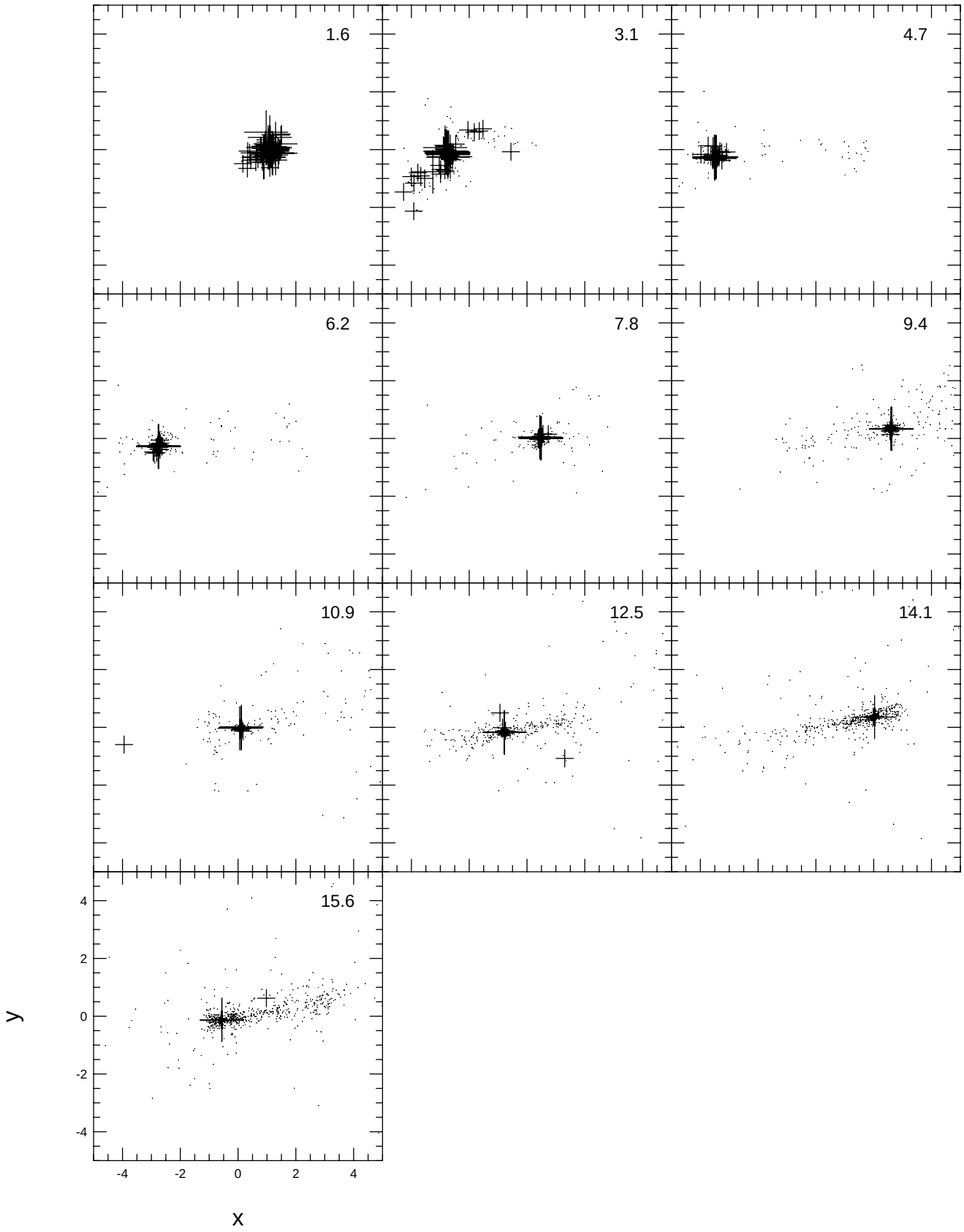

FIG. 10*c*

regarded as a preliminary attempt to extend theoretical understanding to various activities in shell galaxies by considering gas dynamics. The present models are completely self-consistent, modeling both the host and companion galaxies as self-gravitating particle systems. However, we did not focus on the detailed process of shell formation such as investigated by Salmon et al. (1990), partly because the relatively small number of particles employed did not allow a sufficient resolution and a large dynamic range. For example, the shells expected to form in inner regions were not well represented. Instead, the gas dynamics and associated star formation were stressed in the present study. Some important new results obtained here are now discussed in depth.

4.1. "*Poststarburst*" *Nature of Shell Galaxies*

One of the most important results obtained in the present study is that star formation is heavily damped in shell formation. This is because an efficient scattering (dispersal) of the gas cloud system that is indispensable for the formation of shells reduces the density of the gas and hence the star formation rate. This result seems to have the following implication if combined with several observational studies of shell galaxies. Carter et al. (1988) have made photometric and spectroscopic observations of a sample of shell galaxies. They found that the "nucleus" of many shell galaxies shows a spectrum with remarkable Balmer absorption lines, which suggests the dominance of A-type main sequence stars. One possible interpretation is, as they suggest, that those shell galaxies exhibiting A-type-star–dominated spectra are in the poststarburst phase, i.e., several times 10^8 yr after the occurrence of short-period intense star formation. This might seem plausible, because many interacting galaxies, especially those undergoing major mergers, are observed to be experiencing violent star formation along with morphological deformation (see, Larson & Tinsley 1978; Young et al. 1986; Sanders et al. 1988). However, the present numerical study suggests a different possibility. Every case that gives rise to long-lasting regular shell structures was found to lead to efficient suppression of star formation. Therefore, we propose an idea that the "poststarburst" nature of the shell galaxies is not caused by starbursts but a result of truncation of star formation. It should be noted that a spectrum dominated by A-type stars does not necessarily require a preceding starburst but also can result from a sufficiently rapid truncation of star formation. This is well demonstrated in the trajectory of a model galaxy in the plane of Hδ equivalent width versus $B-R$ color. The calculation by Couch & Sharples (1987) indicates that a galaxy whose star formation is suddenly removed moves upward from the initial position on the line occupied by normal galaxies (called the normal line hereafter) as O- and B-type stars start to vanish and then returns down toward the normal line as A-type stars start to die out. In the case of a starburst, however, the galaxy first moves downward from the initial position because of the dominance of newly formed OB stars in early phases and then goes up as these OB stars start to die, passing through the normal line, and finally comes down toward the normal line as A stars die. Carter et al. (1988) indeed showed that those shell galaxies with the sign of a "poststarburst" nature fall on the region above the line delineated by normal galaxies. No shell galaxy is observed below the normal line. However, this fact does not rule out the possibility of starbursts. It may be simply that the starburst takes place too early and has too short a lifetime for shell structures to be developed along with it, preventing these starburst galaxies from being included in a sample of shell galaxies. Our point is that the currently available data do not necessarily require starbursts. It is interesting to note here that Arp (1990) has already pointed out a possibility of suppression rather than enhancement of star formation in violently interacting galaxies, on the ground that such interaction will destroy the gas disk. Although this is not always the case (e.g., we see intense starbursts in the ultraluminous mergers), we should note that the influence of galaxy interaction on the star formation is dependent on the detailed manner in which the galaxies collide.

Two points are worth mention here. One concern is about the spatial extent of the regions that Carter et al. (1988) observed. Because they do not mention the aperture used in their observations, it is not clear how small a region near the nucleus was observed and even whether the nucleus is that of the host elliptical or that of the accreted companion. For this reason, we have checked our numerical results and investigated whether the star formation history is significantly different from place to place in the radial model, run 1. At the epoch of $t = 15.6$, when the shell structure is well developed, we placed a series of concentric annuli with various radii around the elliptical nucleus and analyzed the age distribution of the new stars that are contained in each annulus. The result presented in Figure 11 does not indicate a large difference in the age distribution of new stars at different radii. Every annulus shows a deficiency of stars that have been formed after the first passage of the companion through the elliptical center (i.e., $t > 3$). Therefore, our interpretation of the Carter et al. (1988) observation is unaffected by what aperture size they actually used. It is also noted that the surface density of stars that formed in the initial phase ($0 < t < 3$) increases toward the center of the elliptical, and such a central concentration would be indeed recognized as a nucleus lacking in young stars.

The second point is that the catalog of Malin & Carter (1983), which served as a database for the Carter et al. (1988) study, collects shell galaxies defined in a broad sense, including confused and ill-defined systems (such as loops), in addition to regular ones. It is impossible (at least from Carter et al. [1988] and other available literature) to know how the spectroscopic properties of shell galaxies are correlated with the morphological type of their shell system. Our numerical results suggest that the star formation history in shell galaxies (including those with a confused system) is related to the manner in which the shells are formed and their resultant morphology (§ 3). Unfortunately, it may be difficult to check such correlation observationally because star formation has long ceased regardless of the type of merger when the galaxy develops a shell system and becomes to be classified as a shell galaxy. A poststarburst-like nucleus may be observed in any case.

Other observational results do not permit unique interpretations either. Thronson et al. (1989) show that infrared characteristics of shell galaxies are similar to those of normal-type (mostly S0) galaxies. Their interpretation is that (1) the merger events have no appreciable effects on the star formation process in shell galaxies or (2) the timescale for the creation and maintenance of shells is longer than that for star formation. Wilkinson et al. (1987a) found that the incidence of radio activity in shell galaxies is not signifi-

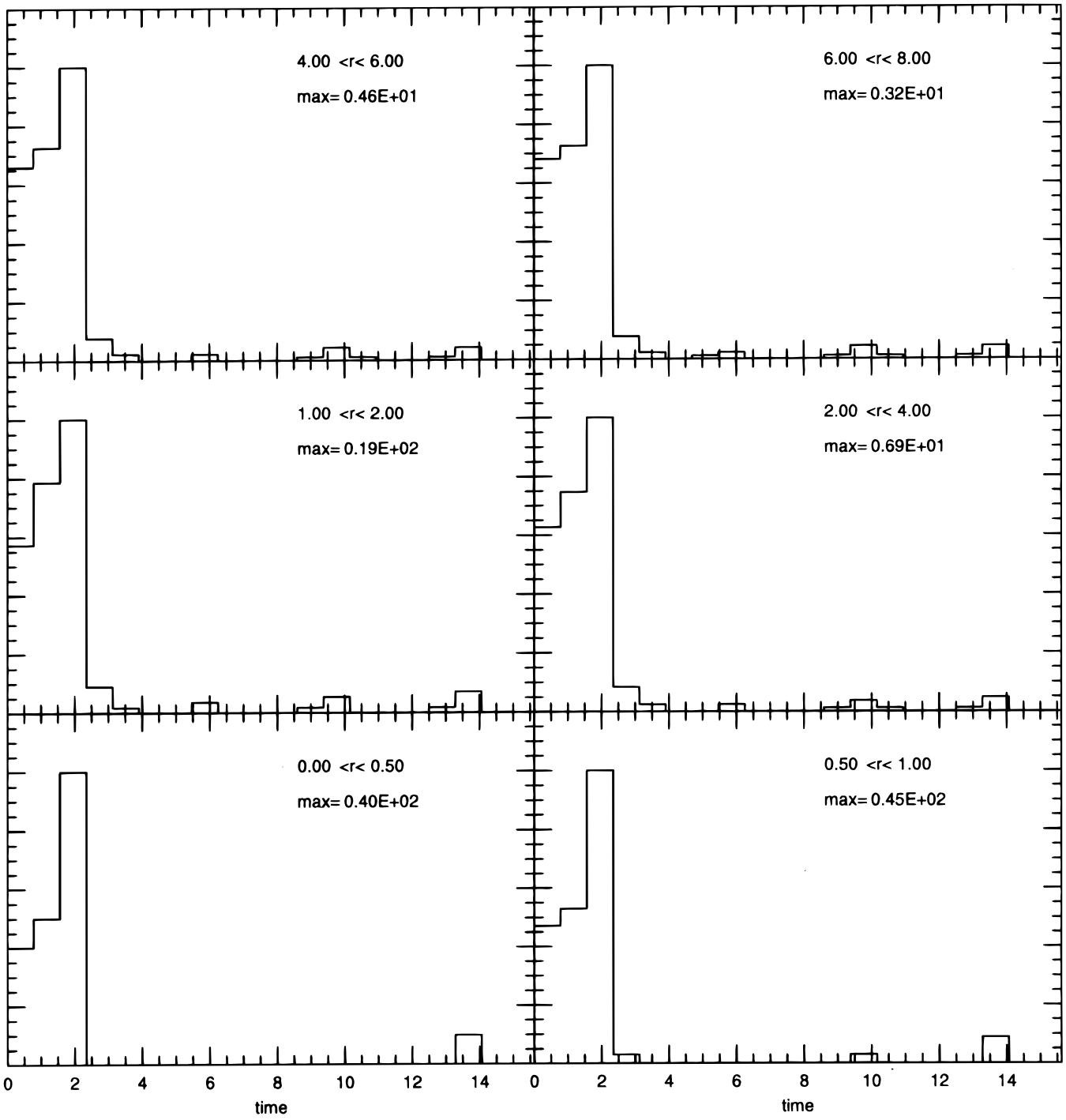

FIG. 11.—Distribution of the birth time for the newly born stars that are located at different projected distances from the center of the elliptical galaxy at the epoch $t = 15.6$ in the radial merger model, run 1. The radial bin is indicated in the upper right of each frame. The ordinate indicates the surface density of the stars with a given birth time (the abscissa) in the given radial bin, obtained when plotted onto the x-y plane. All the histograms are normalized so that they have the same peak height in order to display very low parts in late phases in outer bins. The maximum value of each histogram is given in the upper-right corner of the corresponding frame to facilitate the comparison between different radial bins.

cantly higher than in normal E/S0 galaxies, although there is some evidence that the presence of shells strengthens radio/infrared correlation (Wilkinson, Browne, & Wolstencroft 1987b). In contrast to more systematic but simpler studies such as mentioned above, detailed studies for individual cases are scarce but would be helpful. McGaugh & Bothun (1990) have carried out *UBV* surface photometry of three shell galaxies, Arp 230, NGC 7010, and Arp 223. In the case of Arp 230, the measured colors of the individual shells suggest a burst of star formation in which shell material was involved and which had ceased by the time of complete shell formation. Morphological and photometric evidences, however, suggest that Arp 230 is a product of merger between two spirals and rule out involvement of an elliptical. In the cases of NGC 7010 and Arp 223, shell colors can be explained by passive evolution (aging and segregation) of stellar tidal debris of the companion galaxy accreted by the primary. Therefore, these observations do not seem to present serious contradiction to our numerical results.

4.2. *Gas Dynamics versus Stellar Dynamics*

Although the efficient reduction in star formation rate in shell galaxies is an interesting possibility that the present study has revealed, this result probably depends on the specific model for the interstellar medium adopted. Hernquist & Weil (1992) and Weil & Hernquist (1993) performed a numerical study for sinking satellites that includes interstellar gas components. Their study indicates that the gas is quickly separated from the stellar component of the companion and is accreted to the center of the host spherical galaxy. Their numerical model differs from the present one in two points. First no self-gravity is taken into account in their study. Their companion galaxy is composed of massless particles and falls into the rigid gravitational potential of the host spherical galaxy. Second, they have used the SPH code instead of the inelastic gas cloud model to describe the interstellar gas. This second point, i.e., the difference in the gas model, is considered to be the major cause of difference in the dynamical behavior of the gas. As these authors state, in the SPH, which is meant to describe a continuous fluid, each SPH particle is always feeling the pressure from neighboring particles. When there are two oppositely moving flows, particles from one flow cannot pass through the particles from the other flow. This is exactly the situation that occurs when the gas torn from the companion falls into the center of the host galaxy. When the gas that has fallen first is returning back from the first apocenter passage, it collides with another part of the gas that is about to reach the elliptical center for the first time. Pressure effects mentioned above and energy dissipation (because of the assumption of isothermal state) make the gas condense into a small region at the elliptical center, as discussed in Hernquist & Weil (1992) and Weil & Hernquist (1993). This causes a quick segregation of the gas and the stars. However, a system of discrete gas clouds can behave like a stellar system under certain conditions. A gas cloud system can have a relatively long cloud-cloud collisional timescale depending on the cloud parameters (the cloud size, the mean separation between the clouds, and their velocity dispersion), whereas a continuous gas corresponds to the limit of frequent collisions. Therefore, a system of clouds behaves as an essentially collisionless system, if it experiences a change of the external gravitational field that occurs in a period shorter than the internal cloud-cloud collisional timescale. Such a "quasi-collisionless" nature of the gas cloud system has brought about its morphological similarity to the stellar component and suppression of star formation, especially in the case of the radial merger, as discussed in § 3. A similar difference caused by the adoption of different gas models is reported in Theis & Hensler (1993) for the case of protogalaxy collapse simulations.

The dependence of global gas dynamics on the details of the adopted gas model found here is considered to have an important implication. It is not yet clear which model (discrete or continuous) is a more realistic description of actual interstellar gas. Our knowledge of detailed interstellar gas physics is limited to our Galaxy and a small number of nearby galaxies. The observations done for these galaxies seem to indicate a highly clumpy nature of the interstellar medium, with a large fraction of mass contained in massive discrete clouds of molecular or atomic hydrogen. It is not clear how the physical property of the interstellar gas is altered in abnormal environments such as strongly interacting galaxies, starburst galaxies, and active galaxies. For example, observations of starburst galaxies undergoing mergers have revealed a large-scale emission nebulosity that is not seen in more quiescent galaxies located in isolated environments (e.g., Armus, Heckman, & Miley 1990), suggesting abnormal nature caused by the starbursts. It is not clear whether the observed peculiarity of the interstellar matter (ISM) invalidates the application to these galaxies of a clumpy ISM model such as the one used in the present study. Nevertheless, it will be interesting from a theoretical point of view to investigate systematically the global gas behavior as a function of the "microscopic" physical parameters such as the collisional and dissipational timescales in the gas component.

5. CONCLUSIONS

We have carried out numerical simulations on the accretion of a disk galaxy by a larger elliptical (spherical) galaxy. Both galaxies are constructed by a large number of gravitating particles (more than $\sim 10^4$ particles for each galaxy). A fraction of disk particles in the companion galaxy were made to collide inelastically with each other and form stars depending on the local gas density, mimicking the fundamental behavior of the interstellar gas clouds. Within a limited range of parameters, this study found a relationship, as follows, between the resulting morphology of tidal debris of the satellite and the temporal development of star formation rate.

1. In a radial merger between a large spherical galaxy and a much smaller satellite disk galaxy having 1/10 the mass of the former, star formation activity that had been taking place in the satellite before merger is completely truncated after the first passage of the satellite through the primary center. The stars from the satellite make a system of shells several times 10^8 yr after the cessation of star formation, and this system lasts for more than ~ 1 Gyr. Individual shells are aligned with the direction of the original satellite motion and interleaved in radius on opposite sides of the primary. These stellar shells are accompanied by gaseous shells, which are more diffuse than the stellar ones.
2. A slightly retrograde merger leads to the formation of stellar and gaseous shells that lie near the satellite orbital plane and are located at random position angles around the primary center. This shell system also has a long lifetime ($\gtrsim 1$ Gyr). By the time the shell system starts to develop, star formation is significantly damped.
3. In a slightly prograde merger, a strong starburst is triggered at the nucleus of the tidally deformed satellite galaxy as the satellite approaches the primary. After the starburst has faded out because of depletion of the gas, a system of stellar and gaseous loops encircling the primary center starts to develop.

In sum, for any geometric configuration of a merger, star formation is much reduced by the time a galaxy develops the faint structures that cause it to be classified as a shell galaxy. More important, these results suggest that the "poststarburst" nuclei found in a number of shell galaxies (especially those with a regular shell system) could be a result of truncation of star formation rather than the aftermath of the alleged starburst.

This work is partly based on the first author's (M. K.) Ph.D thesis, which was submitted to Tohoku University in partial fulfillment of the requirements of the doctorate. M. N. is supported by the Scientific Research Grant of the Ministry of Education, Science, and Culture, Japan (07640346).

APPENDIX

DETERMINATION OF DENSITY PEAKS

It was necessary to define the center of each galaxy unambiguously in performing some of the analysis presented in this paper (e.g., Fig. 11). In the present situation, the center of mass of individual galaxies cannot be used because both galaxies can deform greatly. If a few particles are kicked out to large distances from either of the two galaxies, the center of mass of that galaxy can even move out of the main body, thus making the center of mass almost meaningless. Several kinds of centers have been considered to define the center of a N-body system, such as the potential center (Casertano & Hut 1985) and the median position of the particles (McGlynn 1984; Balcells & Quinn 1990).

In order to analyze our simulation data, we have devised the following algorithm to calculate the density peak. First, we set a three-dimensional grid that covers the system. This grid region is divided into $7 \times 7 \times 7$ cells (seven cells in each direction). Second, we count the number of particles contained in each cell. Third, the cell that possesses the maximum particle number is determined. Fourth, all the particles in this cell and the neighboring 26 cells are counted. If this number is below 1/10 of the total particle number, the center of mass of these particles is taken as the density peak. If this condition is not fulfilled, we apply the same procedure to the region covered by the above 27 cells. This procedure is repeated until the condition is satisfied. In making Figure 11, this method was applied to the particles constituting the elliptical galaxy.

REFERENCES

Armus, L., Heckman, T. M., & Miley, G. K. 1990, ApJ, 364, 471
Arp, H. 1990, in Dynamics and Interactions of Galaxies, ed. R. Wielen (Berlin: Springer), 503
Balcells, M., & Quinn, P. J. 1990, ApJ, 361, 381
Barnes, J. E., & Hut, P. 1986, Nature, 324, 446
Carter, D., Prieur, J. L., Wilkinson, A., Sparks, W. B., & Malin, D. F. 1988, MNRAS, 235, 813
Casertano, S., & Hut, P. 1985, ApJ, 298, 80
Couch, W. J., & Sharples, R. M. 1987, MNRAS, 229, 423
Dupraz, C., & Combes, F. 1986, A&A, 166, 53
Fabian, A. C., Nulsen, P. E. J., & Stewart, G. C. 1980, Nature, 287, 613
Fall, S. M., & Efstathiou, G. 1980, MNRAS, 193, 189
Hausman, M. A., & Roberts, W. W. 1984, ApJ, 282, 106
Hernquist, L. 1987, ApJS, 64, 715
———. 1993, ApJS, 86, 389
Hernquist, L., & Quinn, P. J. 1988, ApJ, 331, 682
Hernquist, L., & Weil, M. L. 1992, Nature, 358, 734
Kennicutt, R. C. 1983, ApJ, 272, 54
Kormendy, J. 1977, ApJ, 218, 333
———. 1987, in IAU Symp. 127, Structure and Dynamics of Elliptical Galaxies, ed. T. de Zeeuw (Dordrecht: Reidel), 17
Larson, R. B., & Tinsley, B. M. 1978, ApJ, 219, 46
Levinson, F. H., & Roberts, W. W. 1981, ApJ, 245, 465
Malin, D. F., & Carter, D. 1983, ApJ, 274, 534
McGaugh, S. S., & Bothun, G. D. 1990, AJ, 100, 1073
McGlynn, T. A. 1984, ApJ, 281, 13
Noguchi, M. 1988, A&A, 203, 259
———. 1991, MNRAS, 251, 360
Noguchi, M., & Ishibashi, S. 1986, MNRAS, 219, 305
Prieur, J.-L. 1990, in Dynamics and Interactions of Galaxies, ed. R. Wielen (Berlin: Springer), 72
Quinn, P. J. 1984, ApJ, 279, 596
Richstone, D. O., & Tremaine, S. 1986, AJ, 92, 72
Roberts, W. W., & Hausman, M. A. 1984, ApJ, 277, 744
Rubin, V. C. 1983, in IAU Symp. 100, Internal Kinematics and Dynamics of Galaxies, ed. E. Athanassoula (Dordrecht: Reidel), 3
Salmon, J., Quinn, P. J., & Warren, M. 1990, in Dynamics and Interactions of Galaxies, ed. R. Wielen (Berlin: Springer), 216
Sandage, A., & Visvanathan, N. 1978, ApJ, 223, 707
Sanders, D. B., Soifer, B. T., Elias, J. H., Madore, B. F., Matthews, K., Neugebauer, G., & Scoville, N. Z. 1988, ApJ, 325, 74
Schweizer, F. 1980, ApJ, 237, 303
Seitzer, P., & Schweizer, F. 1990, in Dynamics and Interactions of Galaxies, ed. R. Wielen (Berlin: Springer), 270
Theis, Ch., & Hensler, G. 1993, A&A, 280, 85
Thomson, R. C., & Wright, A. E. 1990, MNRAS, 247, 122
Thronson, H. A., Bally, J., & Hacking, P. 1989, AJ, 97, 363
Toomre, A. 1964, ApJ, 139, 1217
Wallin, J. F., & Struck-Marcell, C. 1988, AJ, 96, 1850
Weil, M. L., & Hernquist, L. 1993, ApJ, 405, 142
Wilkinson, A., Browne, I. W. A., Kotanyi, C., Christiansen, W. A., Williams, R., & Sparks, W. B. 1987a, MNRAS, 224, 895
Wilkinson, A., Browne, I. W. A., & Wolstencroft, R. D. 1987b, MNRAS, 228, 933
Williams, R. E., & Christiansen, W. A. 1985, ApJ, 291, 80
Young, J. S., Kenney, J. D., Tacconi, L., Claussen, M. J., Huang, Y.-L., Tacconi-Garman, L., Xie, S., & Schloerb, F. D. 1986, ApJ, 311, L17